KRONOS FUSION ENERGY

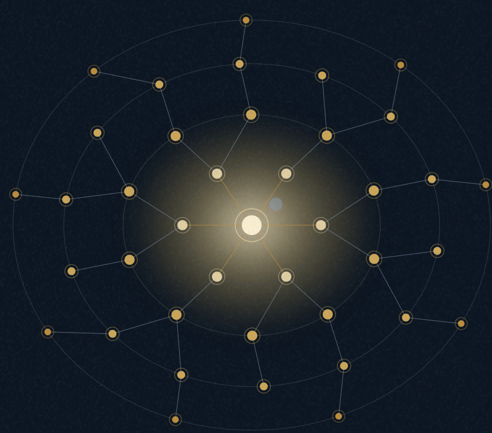

PAPER 2.40 · THE KRONOS 2026 SERIES

Real-Time Detachment Control for a Super-X Divertor in a Compact Spherical-Tokamak Breeder: Radiated-Power-Fraction Regulation with a Radiative-Collapse Guard

A compact, high-power-density spherical-tokamak breeder concentrates its entire exhaust behind a small first wall, and its divertor cannot survive an attached, high-temperature...

Read it live — 3-D model · physics validator · film series

BY P I FORD AND G L KULCINSKI

2026 · EDITORIAL EDITION

THE OFFICIAL RECORD

What this document is, and how to read its numbers

This is a combined editorial. It gathers, in one volume, the two design studies Kronos Fusion Energy released in 2026 — a compact spherical-tokamak tritium/helium-3 breeder and a deuterium–helium-3 tandem-mirror generator — together with the intellectual-property estate, the people, and, in the internal edition, the full commercial case. The scientific text is the same text that appears in the arXiv preprints and the journal submissions; the editorial adds the apparatus a reader needs to hold the whole program at once, and nothing in the physics is altered to fit it.

THE HONESTY STANCE IS THE ASSET

Every headline quantity carries an **evidence class** — DERIVED RECOMPUTED MEASURED REQUIREMENT — and, where a number is a modelled extrapolation rather than a demonstrated value, it is labelled as such and its downside is shown next to it. Several quantities in the underlying corpus moved after first publication; where a value has been withdrawn or restated, the record says so plainly. This is deliberate: a diligence team will find the load-bearing assumptions, so the document surfaces them first.

TWO EDITIONS

This volume is issued in two editions. The **public edition** (light) carries the physics and the design only — no dollar, price, or per-kilogram figure appears anywhere in it. The **internal edition** (dark) adds the economics, the funding architecture, and the defense-commercial analysis, and is marked *Confidential* accordingly; it is not for public distribution. Where the commercial case rests on a modelled assumption rather than a demonstrated one, it is labelled as such and its downside is shown alongside it, on the same terms as the physics.

TITLE	The Kronos Fleet — Hyperion · Aegis · MetroVolt: A Combined Design & Commercialization Study
AUTHOR	Priyanca Ford, Founder & CEO, on behalf of Kronos Fusion Energy
EDITION	2026 Combined Editorial · first issue
COMPANION WORKS	The five-paper arXiv drop — (1) Breeder, (2) Burner, (3) REBCO magnet & tape, (4) Direct Energy Conversion, (5) AI/ML/Quantum control — with matching numbered Zenodo deposits, plus the IOP journal and IAEA-FEC submissions. Patents were filed before the drop.
NAMING	Hyperion = the breeder; Aegis (defense) and MetroVolt (data-center) = one generator in two housings. Internal mode letters (D1, L) do not appear on public surfaces.
STATUS	Conceptual design & simulation study. Nothing herein is a construction commitment.

HOW TO READ THIS VOLUME

The fleet at a glance, and the way its numbers are marked

This volume opens with *Orientation*, presents the five research papers as a bound sequence, and closes with the *Apparatus*. *Foundations* sets out the three general results both machines rest on. *Paper One* is the Hyperion breeder; *Paper Two* the Aegis / MetroVolt generator; *Papers Three, Four and Five* are the enabling science — high-field REBCO magnets and tape, direct energy conversion, and the AI / ML / quantum control stack. A *Digital Twin & 3-D Model* part follows, then the *Environmental* profile. The *Economics* and levelized cost and the *Business Case* and diligence record appear in the internal edition only; the *Simulations* proof record and the Apparatus — patent portfolio, team, limitations, and sources — close both editions.

THE FLEET AT A GLANCE

	HYPERION	AEGIS	METROVOLT
Role	Strategic-isotope foundry	Defense installation power	Campus power
Machine	**Spherical tokamak**	**Tandem mirror**	**Tandem mirror**
Fuel	Deuterium–tritium	Deuterium–helium-3	Deuterium–helium-3
Delivers	Tritium · ^{3}He · 14 MeV n	Resilient installation power	Firm campus power
Physics bar	**Fusion gain only**	Closure (gates named)	Closure + lunar ^{3}He
In the fleet	Breeds the fuel	Proves the generator	Commercial destination

HOW THE NUMBERS ARE MARKED

Every headline quantity carries an evidence class — DERIVED from first principles, RECOMPUTED from raw data, MEASURED in hardware, or a REQUIREMENT yet to be met. Financial figures carry a case label and are confined to the internal (confidential) edition. Values that moved after first publication are shown as withdrawn or restated rather than quietly changed. A capability you can evaluate is one whose limits are on the page.

ABSTRACT

Real-Time Detachment Control for a Super-X Divertor in a Compact Spherical-Tokamak Breeder: Radiated-Power-Fraction Regulation with a Radiative-Collapse Guard

A compact, high-power-density spherical-tokamak breeder concentrates its entire exhaust behind a small first wall, and its divertor cannot survive an attached, high-temperature target: detachment is not an operating option but a design requirement, and holding it at full power against disturbances is a real-time control problem. We formalise that problem for the Hyperion breeder ($P_{\rm fus} = 85.04\,MW$, $B_0 = 8\,T$, $I_p = 9.66\,MA$, negative triangularity $\delta = -0.30$) on a Super-X divertor, and specify the controllers that hold it. From a converged edge-plasma solve (UEDGE) we establish the plant to be controlled: a three-point upstream-density scan drives the target electron temperature from **14.4** eV (attached), through **5.28** eV (marginal), to **1.05** eV (detachment onset), with the divertor-to-upstream density ratio rising to $\mathbf{n_t/n_u = 31.0}$ — within 15 % of an independent one-dimensional arbiter ($\approx$**27**). Scaling the two-point-model onset to the design parallel heat flux $q_{\parallel} \simeq 12\,GW/m^2$ places the deuterium-only detachment density at one-to-two times the Greenwald value: physically inaccessible, so *impurity seeding is mandatory*, and its budget is fixed by coronal cooling curves — argon radiates about 13× harder at the 100 eV edge than in the core, while core tungsten must stay below a tolerance of $0.19\,MW$ per part-per-million to protect the radiation balance. On this demonstrated window we derive three coupled real-time controllers: a detachment-front regulator with two-point-model feedforward, a radiated-power-fraction controller, and a *radiative-collapse guard* cast as a control-barrier-function quadratic program that renders the core-radiation safe set forward-invariant and vetoes any seeding command that would tip the plasma into a radiative collapse. We give the governing equations, the numerical formulation of both the edge solve and the safety-filter QP, and the GPU-HPC campaign that produced every anchor. Reduced-order closed-loop simulations calibrated to the frozen anchors show the front regulator holding the target at 3 eV through a +35 % exhaust-power transient that reattaches the open loop, and the guard capping an over-seed command exactly at the collapse boundary. The one open item is the fully two-dimensional SOLPS-ITER confirmation, which the present UEDGE solve and the one-dimensional arbiter bracket.

Open-access deposit (code & data, CC BY 4.0): DOI 10.5281/zenodo.22645874 · Zenodo community *kronos_fusion_energy*. Explore it live: interactive 3-D model · physics validator.

Keywords: detachment · Super-X divertor · radiated-power fraction · impurity seeding · control-barrier function · radiative collapse · UEDGE · spherical-tokamak breeder

CONTENTS

Table of Contents

NOMENCLATURE

Symbols, units, and the names of things

Q	plasma (fusion) gain, P_{fus}/P_{aux}
Q_E	engineering gain, net electric out / recirculating in
H_{98}	confinement enhancement over the IPB98(y,2) scaling
Z_{eff}	effective ion charge
c_{ee}	electron–electron bremsstrahlung leading coefficient, 2.120022 (exact)
τ_E	energy confinement time
I_p	plasma current
R_0, a	major radius, minor radius
κ, δ	elongation, triangularity
β_N	normalized plasma beta (Troyon-normalized)
TBR	tritium breeding ratio
DEC	direct energy conversion
CF	plant capacity factor (availability)
FOAK / NOAK / BOAK	first / n^{th} / best of a kind
Hyperion	the ST breeder (internal: Mode D2)
Aegis	the generator, defense/installation housing (internal: Mode M)
MetroVolt	the generator, data-center housing (Mode M)

detachment; Super-X divertor; radiated-power fraction; impurity seeding; control-barrier function; radiative collapse; UEDGE; spherical-tokamak breeder

Official version: https://www.kronosfusionenergy.com/publications/real-time-detachment-control-for-a-super-x-divertor-in-.html

§ 1

Introduction

THE EXHAUST PROBLEM IN A COMPACT SPHERICAL-TOKAMAK BREEDER

A spherical tokamak (ST) confines a large plasma current in a small volume, which is exactly what makes it an attractive compact neutron source and tritium breeder [1,2,3] and, at the same time, what makes power exhaust its most concentrated engineering stress. The Hyperion breeder puts $P_{\text{fus}} = 85.04\,MW$ of fusion power behind a first wall at major radius $R_0 = 1.20\,m$, holds $I_p = 9.66\,MA$ behind a centrepost magnet at a peak field of 16.84 T, and operates in a negative-triangularity ($\delta = -0.30$) regime chosen for good confinement without an edge pressure pedestal or the associated edge-localised-mode cycle [4,5]. The scrape-off layer (SOL) funnels the exhaust power into a narrow channel; with a near-SOL power fall-off length set by the poloidal field [6,7], an attached, high-temperature divertor target in this device would see a surface heat flux orders of magnitude above the tens-of-MW/m^2 that any plasma-facing material can survive.

Detachment — deliberately cooling the target plasma below a few electron-volts so that momentum and power are shed volumetrically in the divertor volume before they reach the strike point [8,11,9] — is the accepted route out of that impasse. In a compact ST breeder detachment is not merely desirable; it is a hard requirement of the design point, because the unmitigated target load exceeds the material limit by two orders of magnitude. Two further design choices widen the window in which detachment can be held. First, a *Super-X* divertor routes the outer leg to a large target major radius with high total flux expansion and a long parallel connection length, lowering the geometric heat-flux concentration and enlarging the volume available for volumetric losses [15]. Second, impurity *seeding* converts a controlled fraction of the exhaust power into line radiation upstream of the target [12,16]. Neither is a set-and-forget lever: the detached state is a narrow, disturbance-sensitive operating point that must be actively held.

DETACHMENT AS A CONTROL PROBLEM

Holding detachment against transients has become a discipline of its own. Kallenbach and co-workers demonstrated divertor power-load feedback via nitrogen seeding on ASDEX Upgrade [13] and framed the general impurity-seeding exhaust problem from present devices to DEMO [12]. Ravensbergen *et al.* closed a real-time feedback loop on the location of the impurity emission front on TCV, using multispectral imaging to reconstruct the front position and a system-identified controller to hold it, with front-response times of tens of milliseconds [14]. Verhaegh *et al.* quantified the detachment physics of a genuine Super-X divertor on MAST Upgrade, isolating the plasma–molecule interactions that dominate the particle and power balance deep in detachment [15]. Across these results a common structure appears: a scalar detachment observable (target temperature, front position, or radiated fraction), a seeding or fuelling actuator with tens-of-millisecond dynamics, and a safety concern that the same actuator, pushed too hard, drives the core into a radiative collapse.

Two ingredients are missing for a compact nuclear ST breeder. The first is a controller set derived from, and gated against, a *converged* edge solve for the specific device rather than a generic scaling. The second is an explicit *safety* layer: a certified filter that keeps the seeded plasma inside the region where the core radiation balance is stable, so that a detachment or radiated-fraction command can never, even transiently, request a collapse. Control-barrier functions (CBFs) provide exactly such a filter with a forward-invariance guarantee [26], and reference/command governors provide the constrained arbitration between competing set-point demands on a shared actuator [27]; neither has been reduced to practice for divertor radiative-collapse protection.

CONTRIBUTION

This paper does two things. It *establishes the plant* from converged edge physics — how detachment is reached on the breeder Super-X divertor, why deuterium alone cannot reach it at design power, and what impurity budget seeding must respect (§2) — and it *specifies and demonstrates the controllers* that hold the resulting window (§3). Specifically we contribute: (i) a governing-equation treatment of the Super-X SOL, the two-point detachment model, the Lengyel impurity-radiation integral, and the coronal radiation budget, cast as the formal constrained-regulation problem the controllers solve (§2); (ii) three coupled controllers — a detachment-front regulator with a two-point-model feedforward gain, a radiated-power-fraction controller, and a radiative-collapse guard formulated as a control-barrier quadratic program with a proof of forward-invariance of the core-radiation safe set (§3); (iii) the numerical formulation of both the finite-volume edge solve and the real-time safety-filter QP, with convergence and latency (§4); (iv) the GPU-HPC campaign, naming the codes run for this paper (§5); and (v) results including reduced-order closed-loop demonstrations of the front regulator and the guard (§6), a quantitative comparison to the published detachment-control and impurity-tolerance literature (§7), and one honest open item (§8). Every quantitative claim traces to a frozen result in the Kronos Physics De-Risking Register [36]; serial identifiers (e.g. BR-L2-A21) are given inline so each number is auditable.

§ 2

Governing equations and the formal problem

THE SUPER-X SCRAPE-OFF LAYER AND THE PARALLEL HEAT FLUX

The exhaust power P_{SOL} that survives core radiation enters a SOL channel of poloidal width λ_q mapped to the outboard midplane. The peak parallel heat-flux density at the entrance to the divertor leg is

$$q_\parallel = \frac{P_{\mathrm{SOL}}}{2\pi R\,\lambda_q\,\sin\theta_\wedge}\,f_x^{-1},$$

where R is the flux-surface major radius, $\theta_\wedge$ the field-line pitch at the target, and $f_x \geq 1$ the total flux expansion between midplane and target. The near-SOL width follows the multi-machine scaling $\lambda_q \propto B_{\mathrm{pol}}^{-1}$ [6], so a high-current compact ST has an intrinsically narrow channel and a large $q_\parallel$. The Super-X geometry attacks equation (1) directly: routing the outer strike point to a large target radius R_t raises $2\pi R_t$ and raises f_x, and tilting the plate lowers $\sin\theta_\wedge$, so the projected surface load $q_{\perp,t} = q_\parallel \sin\theta_\wedge / f_x$ is reduced by a large geometric factor relative to a conventional short leg (figure 1). For the breeder the design upstream value used throughout is $q_\parallel \simeq 12\,GW/m^2$.

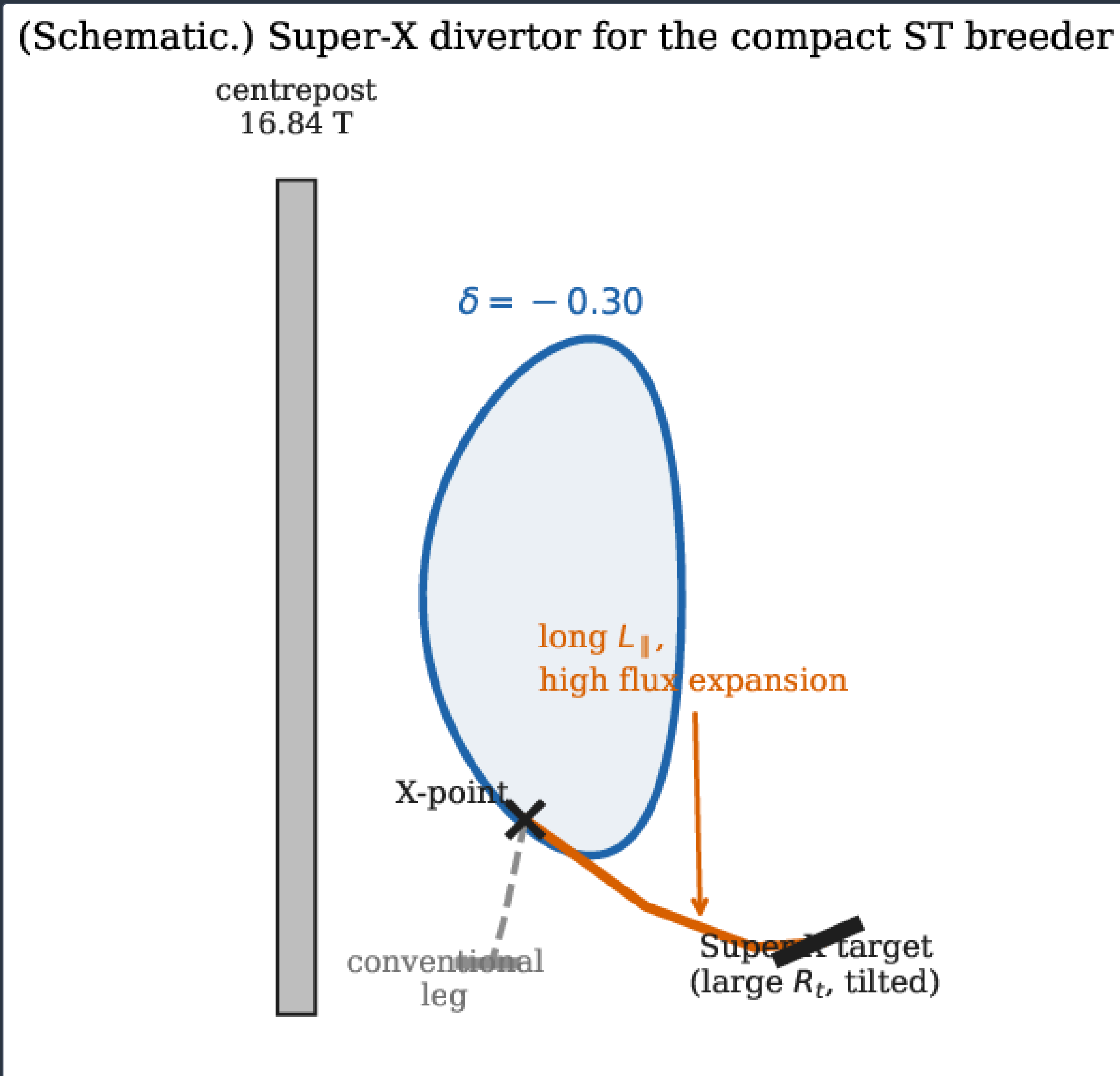

(Schematic.) The Super-X divertor for the compact ST breeder. The outer leg is routed to a large target major radius R_t with high total flux expansion and a long parallel connection length $L_\parallel$, lowering the geometric heat-flux concentration of equation (1) relative to a conventional leg (dashed) and enlarging the volume available for the volumetric losses that produce detachment. Negative triangularity $\delta = -0.30$ and the 16.84 T centrepost are indicated. No data values are shown.

THE TWO-POINT DETACHMENT MODEL

Along a field line of parallel length $L_\parallel$, electron parallel heat conduction obeys the Spitzer–H\"arm closure $q_\parallel = -\kappa_{0e} T_e^{5/2}\, \mathrm{d}T_e/\mathrm{d}s$ with [redacted]. Integrating from target (s=0, $T_{e,t}$) to upstream (s=$L_\parallel$, $T_{e,u}$) with the power deposited near the target gives the conduction relation

$$T_{e,u}^{7/2} \;=\; T_{e,t}^{7/2} \;+\; \frac{7}{2}\,\frac{q_\parallel\, L_\parallel}{\kappa_{0e}},$$

so $T_{e,u} \propto (q_\parallel L_\parallel)^{2/7}$ when $T_{e,t} \ll T_{e,u}$. Total pressure balance between the two points, allowing a momentum-loss fraction f_{mom} to charge-exchange and recombination, reads

$$2\, n_t T_{e,t} \;=\; \big(1 - f_{\mathrm{mom}}\big)\, n_u T_{e,u},$$

and the target heat flux carried by the sheath at heat-transmission coefficient $\gamma \approx 7$ is $q_t = \gamma\, n_t T_{e,t}\, c_{s,t}$ with $c_{s,t} \propto T_{e,t}^{1/2}$. Eliminating n_t and writing the fraction of upstream power radiated or otherwise lost before the target as f_{rad} yields the target-temperature scaling

$$T_{e,t} \;\propto\; \frac{q_\parallel^{10/7}\, L_\parallel^{-4/7}}{n_u^2\,(1 - f_{\mathrm{mom}})^2}\, \big(1 - f_{\mathrm{rad}}\big)^2,$$

the familiar $T_{e,t} \propto n_u^{-2}$ collapse [8,9]. Detachment onset is the crossing of a target-temperature threshold $T_{e,t} \le T_{\mathrm{det}}$, empirically $T_{\mathrm{det}} \approx 5\, eV$ [9], at which volumetric momentum loss switches on strongly and the target ion flux rolls over [11,15]. Setting $T_{e,t} = T_{\mathrm{det}}$ in equation (4) at fixed loss fractions gives the detachment upstream density,

$$n_{u,\mathrm{det}} \;\propto\; q_\parallel^{5/7}\, L_\parallel^{-2/7},$$

the scaling used below to project the measured onset to design power.

THE MEASURED DETACHMENT WINDOW

Equations (2)–(5) are the reduced skeleton; the plant is established by a converged two-dimensional edge solve. A UEDGE [20] SOL solve scoped to the breeder ($B = 8\,T$, poloidal field 2.76 T, $L_\parallel \approx 6.5\,m$, plate recycling 0.98) was advanced to true steady state at three upstream densities (serial BR-L2-A21). The target temperature collapses monotonically as core density rises (table 1, figure 2): from an attached 14.4 eV, through a marginal 5.28 eV sitting on the 5 eV threshold, to a cold 1.05 eV at detachment onset, where the divertor-to-upstream density ratio reaches $n_t/n_u = 31.0$. That onset ratio agrees with an independent one-dimensional two-point arbiter ($\approx$27) to within 15 %, and the collapse follows the $T_{e,t} \propto n_u^{-2}$ trend of equation (4), steepening into onset as neutral momentum loss switches on.

n_{core} (/M³)	$n_{e,u}$ (/M³)	$T_{e,u}$ (EV)	$T_{e,t}$ (EV)	n_t/n_u	STATE
1×10^{20}	6.05×10^{19}	106.0	14.4	15.2	attached
2×10^{20}	1.11×10^{20}	84.9	5.28	19.9	marginal (at threshold)
4×10^{20}	1.96×10^{20}	66.7	1.05	31.0	detachment onset

Converged UEDGE upstream-density scan for the breeder Super-X SOL (BR-L2-A21). The target temperature collapses through the §I5

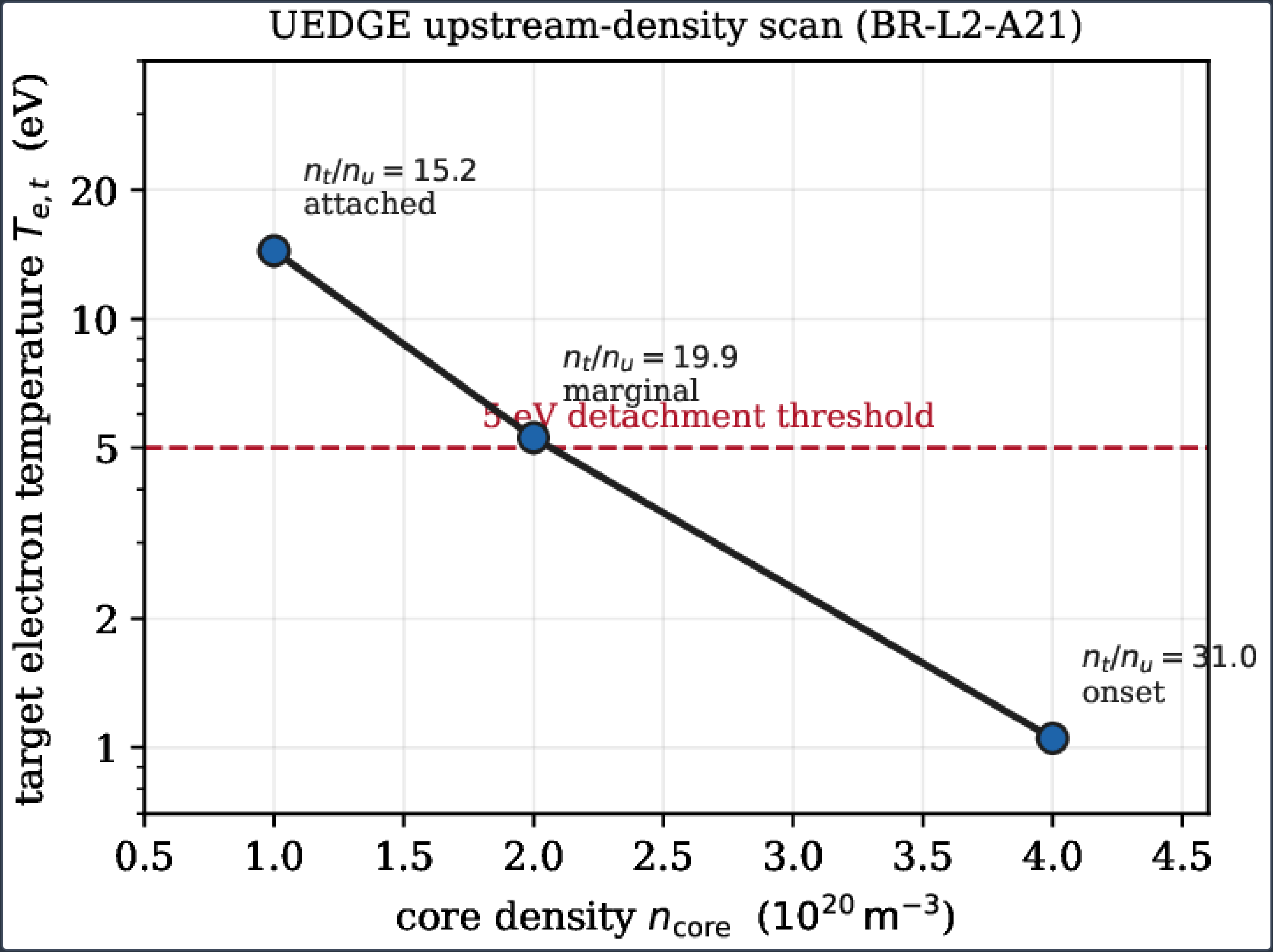

Target electron temperature versus core density from the converged UEDGE scan (BR-L2-A21). The solution crosses the 5 eV detachment threshold (dashed) between $n_{\text{core}} = 2$ and $4e20\,/m^3$; the divertor-to-upstream density ratio n_t/n_u is annotated at each point. This is the plant the controllers of §3 must hold.

The decisive result follows from equation (5). Scaling the measured onset from the scoped scan to the design parallel heat flux $q_\| \simeq 12\,GW/m^2$ places the deuterium-only detachment density at one-to-two times the Greenwald limit $n_{\text{GW}} = I_p/(\pi a^2) \approx 1.3e21\,/m^3$ (with minor radius $a = R_0/A = 0.48\,m$), an operating point above the density limit and therefore physically inaccessible (figure 3); the companion Greenwald-limit and radiative-boundary study maps this envelope in full [31]. Density alone cannot detach the breeder Super-X divertor at design exhaust: *impurity seeding is mandatory*. This converts the exhaust problem from “can we detach?” to “how do we hold seeded detachment steady while protecting the core?”, which is the control problem of §3.

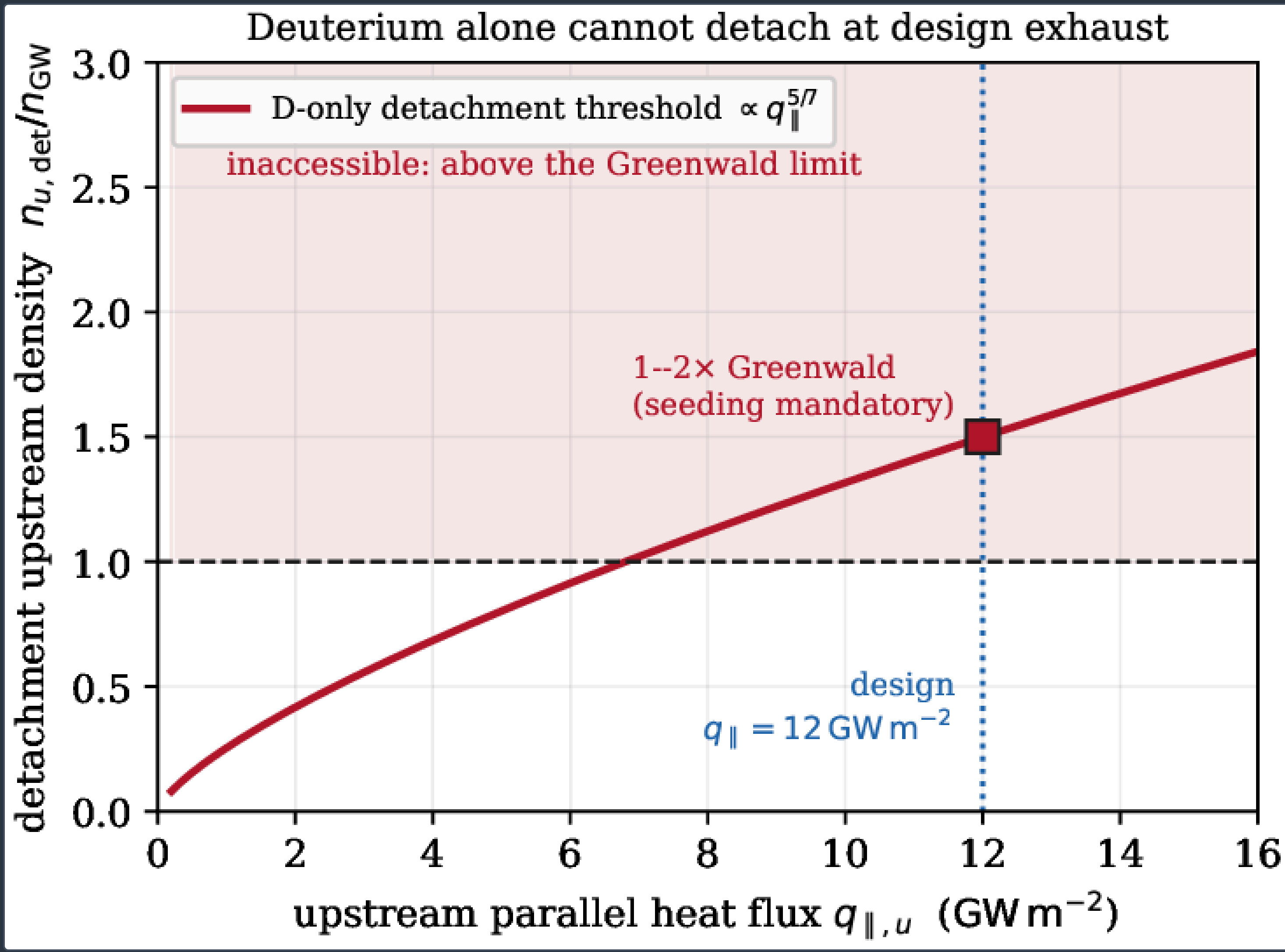

Two-point-model detachment threshold, equation (5), scaled from the frozen onset to design exhaust. At $q_\parallel \simeq 12\,GW/m^2$ the deuterium-only detachment density lands at one-to-two times Greenwald (shaded, inaccessible), so seeding is mandatory. The curve exponent $5/7$ is analytic; the 1–$2\times$ Greenwald band at the design point is the frozen conclusion of BR-L2-A21.

THE IMPURITY-RADIATION BUDGET: THE LENGYEL INTEGRAL AND THE TUNGSTEN TOLERANCE

Seeding must radiate power at the edge without poisoning the core. The parallel-integrated radiated power set by a seeded impurity of concentration $c_z = n_z/n_e$ follows the Lengyel model [19,12]: combining the conduction equation with the radiation source $Q_{\mathrm{rad}} = c_z n_e^2 L_z(T_e)$, where L_z is the coronal cooling function, the upstream heat flux that can be dissipated is

$$q_\parallel \;=\; \left[\,2\,\kappa_{0e}\,\left(n_u T_{e,u}\right)^2 \int_{T_{e,t}}^{T_{e,u}} c_z\,L_z(T)\,T^{1/2}\,\frac{\mathrm{d}T}{T^2}\,\right]^{1/2},$$

so the seed concentration required to radiate a target fraction of the exhaust scales as $c_z \propto q_\parallel^2/(n_u^2\mathcal{I}_z)$ with $\mathcal{I}_z = \int L_z T^{-3/2}\mathrm{d}T$ the cooling integral over the radiating layer. The choice of radiator is fixed by where L_z peaks. Coronal-equilibrium cooling curves (serial BR-L2-A29, radas/ColRadPy over ADAS ADF11 data [17,18]; the full collisional-radiative treatment is the companion impurity-radiation study [30]) give the two anchors that decide the budget (figure 4): argon's cooling function is small in the core ($L_z^{\mathrm{Ar}} = 1.45e-33\,Wm^3$ at 15 keV) and rises about $13\times$ toward the 100 eV edge, so argon radiates where it is wanted and not where it is not; tungsten radiates hard everywhere ($L_z^{\mathrm{W}} = 5.70e-32\,Wm^3$ at 15 keV, mean charge $\langle Z\rangle \approx 62$) and is the species to fear.

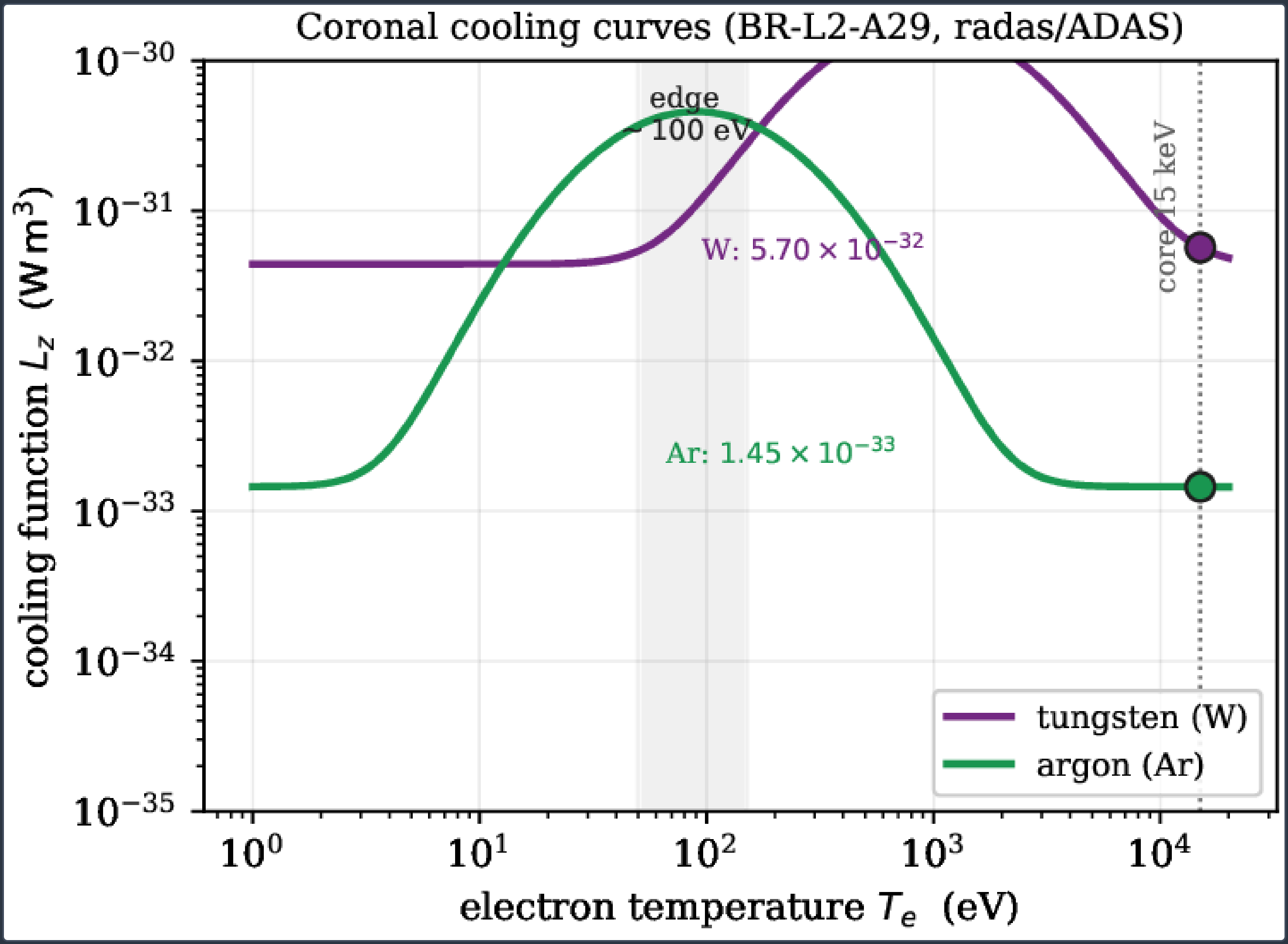

Coronal-equilibrium cooling functions for argon and tungsten (BR-L2-A29, radas/ADAS). Filled markers are the frozen anchor values at 15 keV; the curves are the representative coronal shapes anchored to those values, showing argon's $\sim 13\times$ core-to-edge contrast that makes it the edge radiator and tungsten's flat, high loss that makes it the core poison.

Quantitatively, the tungsten radiated-power add-on is $\Delta P_{\text{rad}} = c_W \langle n_e^2 L_z^{\text{W}} \rangle V_{\text{core}} \approx 0.19\, MW$ per part-per-million of core tungsten (figure 5). Holding $c_W \leq 3$ keeps the tungsten add-on below 0.57 MW — under $13\,\%$ of the register core radiation budget $P_{\text{rad}} = 4.670\, MW$, of which bremsstrahlung is 3.117 MW and synchrotron 1.553 MW (Zeff $= 1.158$; independently re-run here). The radiated-fraction controller therefore has two demands that pull in opposite directions — inject enough argon to detach, and keep tungsten scarce enough not to over-radiate the core — and the atomic data set the numeric guard-rails for both.

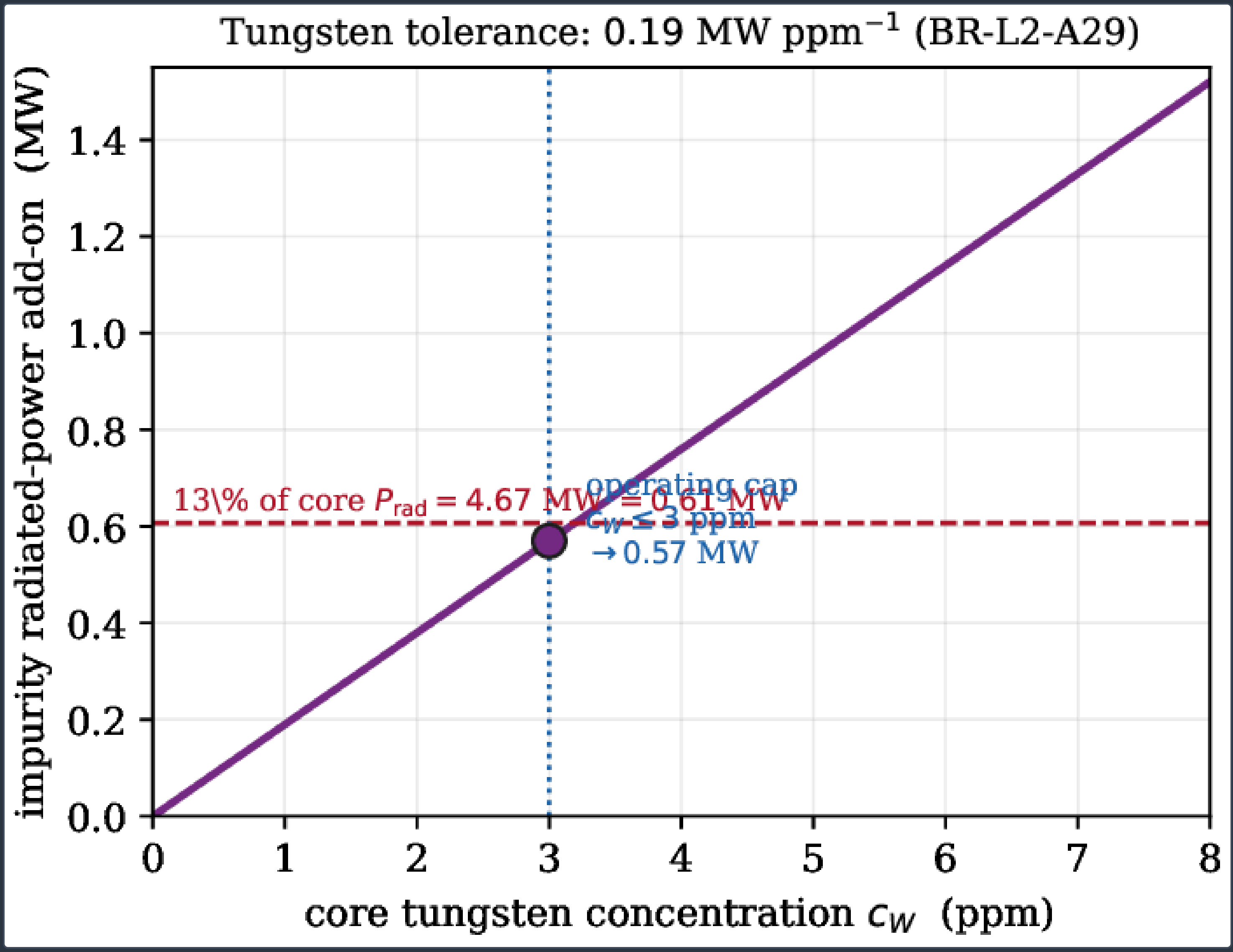

Core tungsten tolerance (BR-L2-A29). The impurity radiated-power add-on is linear in core tungsten concentration at 0.19 MW per ppm; the operating cap $c_W \leq 3$ holds the add-on below $13\,\%$ of the 4.670 MW core radiation budget (dashed).

GEOMETRY AND HEAT-FLUX MARGIN

Two geometric levers set the margin the controllers act against (figure 6). A reduced 2-D edge model of the Super-X leg (serial HX-14, SOLPS-ITER proxy with an Eich near-SOL width $\lambda_q \approx 0.21\,mm$ and $q_{\|} \approx 27.4\,GW/m^2$ at the target projection) gives an unmitigated peak target load of 1370 MW/m² for a conventional leg versus 171 MW/m² for the Super-X leg — the geometric factor of equation (1) alone is an 8× reduction — and a further radiative dissipation of $\sim 94\,\%$ brings the Super-X target below the 10 MW/m² material limit, with detachment ($T_{e,t} \leq 5\,eV$) reached near $91\,\%$ dissipation. Independently, a double-null equilibrium (serial BR-CX-02, FreeGS) splits the exhaust over two targets and drops the peak *surface* heat flux from 8.0 to 4.4 MW/m² (1.8× lower) relative to single-null. Stacking the levers walks the required core argon seed fraction down a ladder — from $6.4\,\%$ for a single lever, through $2\text{–}3\,\%$ for Super-X and $\sim 1\,\%$ adding double-null, to a core-tolerable $\leq 0.5\,\%$ adding a snowflake corner (serial BR-L2-A11-SUM; the stacked closure reproduced by a Monte-Carlo of $N = 4000$ in BR-SX-09). The geometric down-select behind this ladder is the companion stacked-detachment-portfolio study [29], and a flowing-lithium vapour-box leg is the companion alternative exhaust path [33]. The controllers therefore hold a window that geometry has already widened.

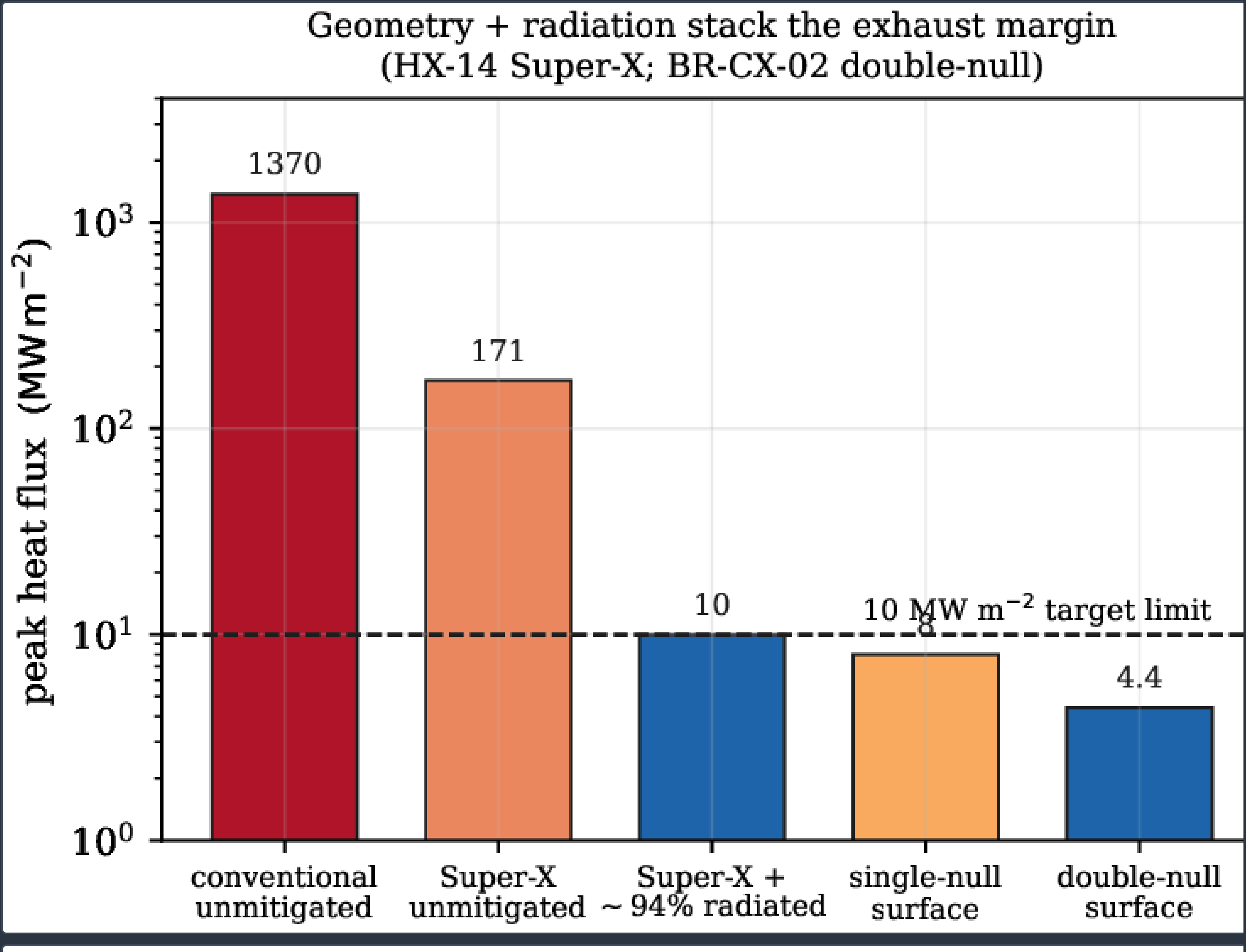
Geometry + radiation stack the exhaust margin
(HX-14 Super-X; BR-CX-02 double-null)
peak heat flux (MW m⁻²)
1370
171
10
10 MW m⁻² target limit
8
4.4
conventional unmitigated
Super-X unmitigated
Super-X + ~ 94% radiated
single-null surface
double-null surface

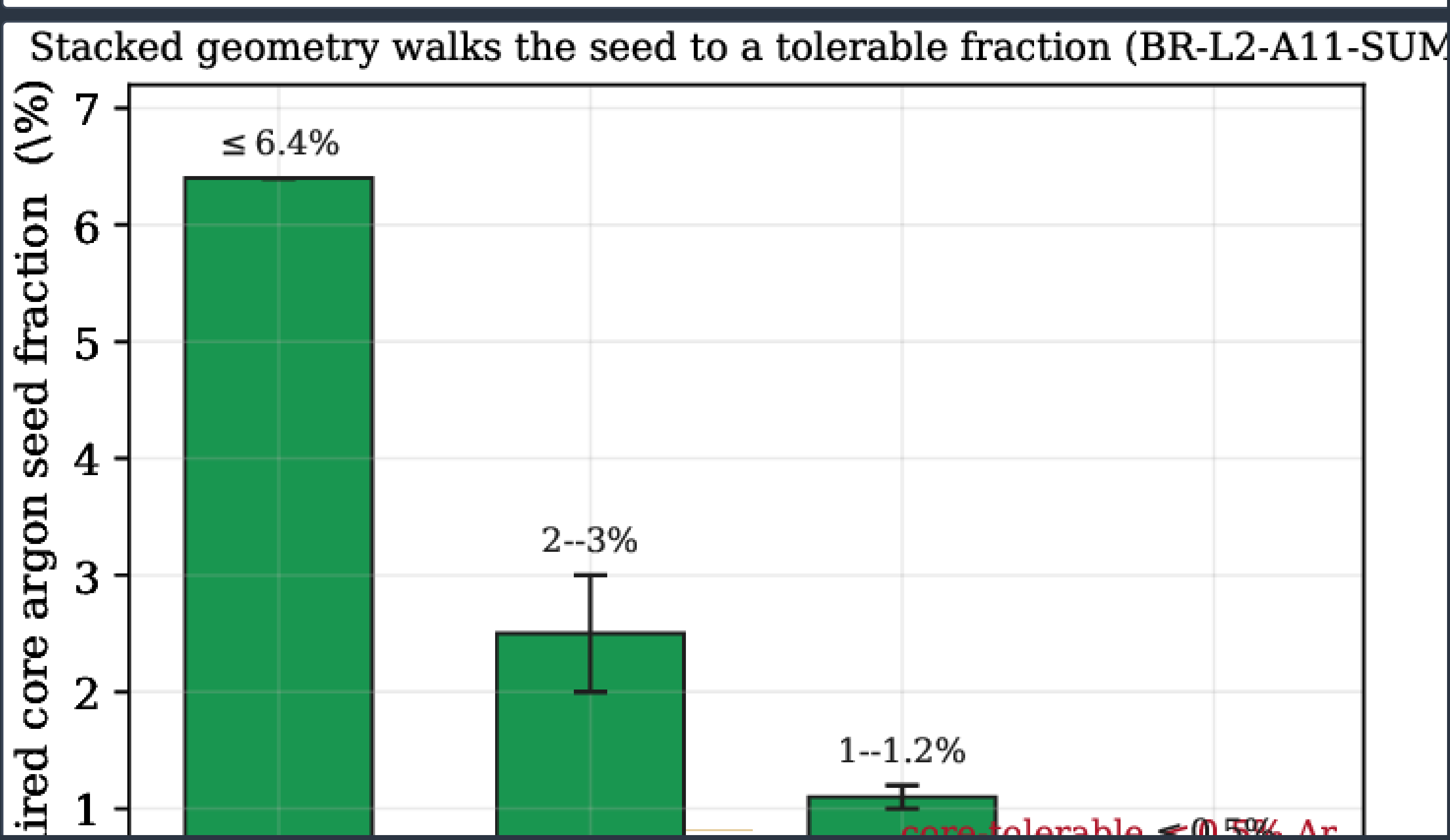
Stacked geometry walks the seed to a tolerable fraction (BR-L2-A11-SUM
ired core argon seed fraction (\%)
≤ 6.4%
2--3%
1--1.2%
core tolerable ≤ 0.5% Ar

THE FORMAL CONTROL PROBLEM

Collecting the physics, the exhaust state to be regulated is

$$x = \left(T_{e,t},\ f_{\mathrm{rad}},\ P_c\right)^\top,$$

where $T_{e,t}$ is the target temperature (a proxy for detachment depth / front position), f_{rad} the divertor-dissipated power fraction, and P_c the core radiated power. The actuators are $u = (\Gamma_{\mathrm{Ar}},\ \Gamma_{\mathrm{D_2}},\ u_{\mathrm{sw}})^\top$: the argon seeding rate, a deuterium fuelling/puff rate, and a strike-point sweep amplitude. The regulated outputs are $T_{e,t}$ and f_{rad}; the constraints are the safety envelope

$$\begin{aligned} T_{e,t} &\le T_{\mathrm{det}} = 5\,\mathrm{eV} && \text{(stay detached)},\\ P_c &\le P_{\mathrm{collapse}} && \text{(no radiative collapse)},\\ q_{\perp,t} &\le q_{\mathrm{lim}} = 10\,\mathrm{MW/m^2} && \text{(target survival)},\\ c_W &\le 3 && \text{(tungsten guard)}. \end{aligned}$$

Equation (8) is the load-bearing safety constraint: the argon actuator that produces detachment (8) and radiated fraction is the same actuator that, over-driven, violates (8). The problem is thus a constrained regulation of $(T_{e,t}, f_{\mathrm{rad}})$ on a shared actuator whose authority is bounded by a certified safe set, which is what §3 builds.

§ 3

The exhaust control complement

The physics of §2 defines a demonstrated operating window; three coupled controllers hold it, behind a certified safety clamp and gated by explicit acceptance tests, in the maturity-gated pattern used across the Kronos control architecture (figure 7). Each is a supervisory (L4) controller that reads a validated real-time state estimate — the same class of real-time reconstruction and physics-model-in-the-loop pipeline that underlies modern tokamak equilibrium and profile control [23,24] — and emits a clamped seeding/fuelling command, never a direct actuation outside the certified safe set. The complement is complementary to, not a competitor of, learned policy control [25]: a learned policy can act on the guarded, arbitrated set-points below rather than on the raw telemetry. Table 2 lists the complement.

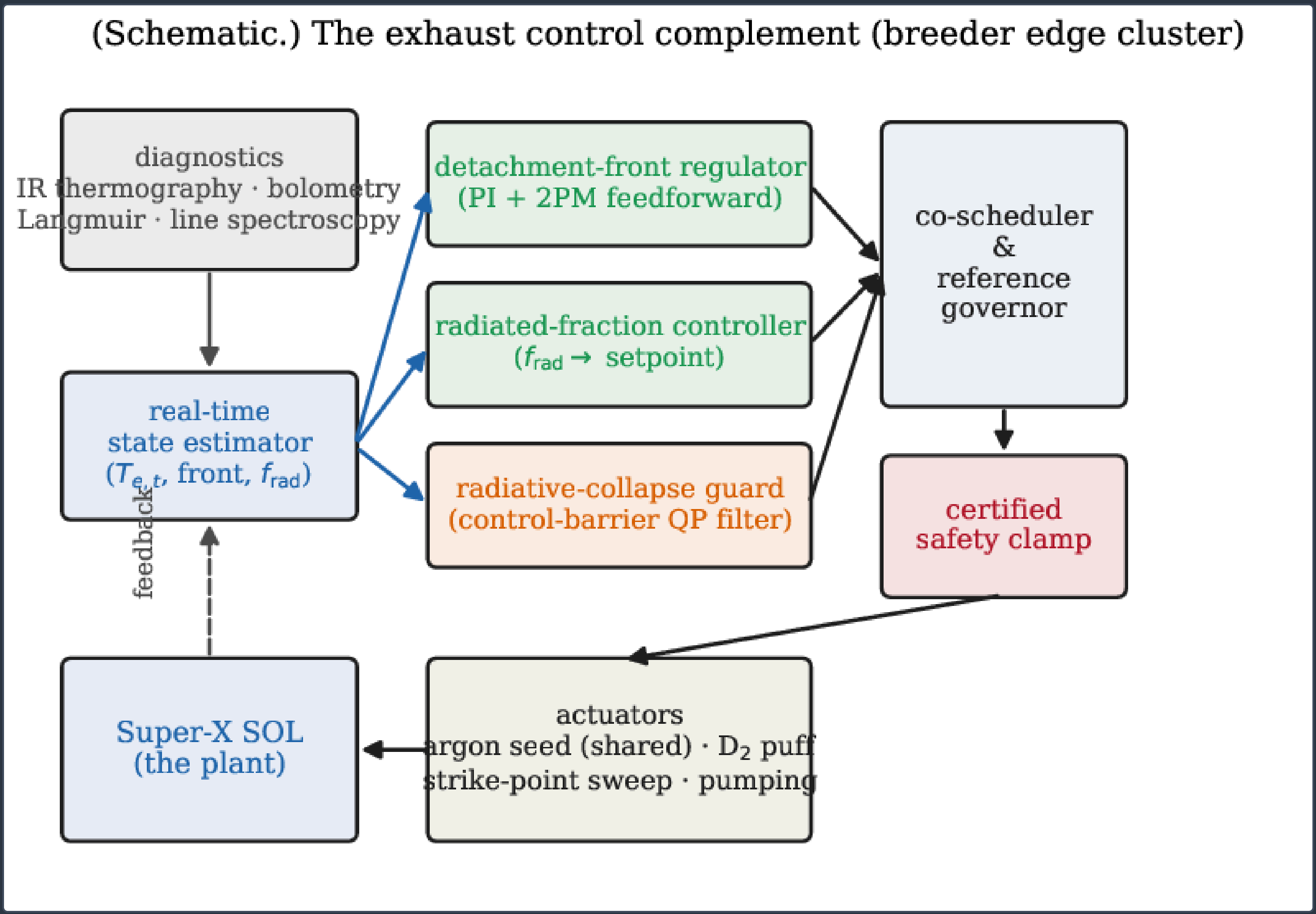

(Schematic.) The breeder exhaust control complement. A real-time state estimator fuses IR thermography, bolometry, Langmuir and line-spectroscopy telemetry into $(T_{e,t}, \text{front}, f_{rad})$; the detachment-front regulator and radiated-fraction controller share the argon actuator and are arbitrated by a reference governor; the radiative-collapse guard is a control-barrier QP that projects every seeding command into the core-radiation safe set before it reaches the certified safety clamp and the plant. Structure only; no data values.

DETACHMENT-FRONT REGULATOR

The primary controller regulates the target temperature (equivalently the impurity emission-front position) to a set-point $T^*_{e,t}$ chosen safely below threshold, e.g. $T^*_{e,t} = 3\,eV$. Linearising the static two-point map (4) about the operating point gives the feedforward sensitivity of target temperature to seeding through the radiated fraction,

$$\frac{\partial T_{e,t}}{\partial \Gamma_{\rm Ar}} = \frac{\partial T_{e,t}}{\partial f_{\rm rad}}\,\frac{\partial f_{\rm rad}}{\partial \Gamma_{\rm Ar}} = -\,2\,\frac{T_{e,t}}{1-f_{\rm rad}}\,\frac{\partial f_{\rm rad}}{\partial \Gamma_{\rm Ar}},$$

which is negative and grows as $f_{\rm rad} \to 1$ — the plant becomes more seed-sensitive the deeper it detaches, so a fixed-gain loop would go unstable near onset. The regulator therefore combines this analytic feedforward with a proportional-integral (PI) feedback and back-calculation anti-windup [28]:

$$e(t) = T_{e,t}(t) - T^*_{e,t},$$
$$\Gamma^{\rm cmd}_{\rm Ar}(t) = \Gamma^0_{\rm Ar} + K_p\,e(t) + K_i\int_0^t e(\tau)\,\mathrm{d}\tau + \Delta\Gamma_{\rm aw},$$

with the anti-windup term $\Delta\Gamma_{\rm aw} = T_t^{-1}\int(\Gamma^{\rm sat} - \Gamma^{\rm cmd})$ returning the integrator whenever the seed saturates. The front dynamics are well approximated by a first-order response of transport time $\tau_T \sim 5\,ms$ (parallel transit plus gas response), consistent with the tens-of-millisecond front-response times reported on TCV [14], and the loop is tuned for a closed-loop bandwidth well inside that limit. The acceptance test is that the target stays detached ($T_{e,t} \le T_{\rm det}$) across the disturbance set.

RADIATED-POWER-FRACTION CONTROLLER

Detachment depth and total radiated fraction are distinct set-points served by the same argon valve, so a second loop regulates $f_{\rm rad}$ to a target $f^*_{\rm rad}$ in the 0.90–0.94 dissipation window established in §2.5 (HX-14/HX-15). Its plant is again first-order, $\tau_f\,\dot{f}_{\rm rad} = -f_{\rm rad} + f^{\rm ss}_{\rm rad}(\Gamma_{\rm Ar})$ with $f^{\rm ss}_{\rm rad} = 1 - \exp(-\beta\,\Gamma_{\rm Ar})$ from equation (6), and its controller a PI with the same anti-windup. Because the two loops share the argon actuator, they are co-scheduled by a reference governor [27] that solves, each tick, a small constrained arbitration

$$\min_{r\in\mathcal{R}} \left\| \quad r - \quad r_{\rm des} \right\|^2 \quad \text{s.t.} \qquad x(\quad r) \in \mathcal{C},$$

choosing the closest admissible pair of set-points $r = (T^*_{e,t}, f^*_{\rm rad})$ to the operator demand $r_{\rm des}$ that keeps the predicted state in the safe set $\mathcal{C}$ of equations (8)–(8). The acceptance test is that $f_{\rm rad}$ is held within tolerance of its set-point across the operating range.

THE RADIATIVE-COLLAPSE GUARD AS A CONTROL-BARRIER FILTER

The safety layer is the load-bearing novelty. Over-seeding argon raises the core radiation P_c; if P_c approaches the heating power the core cools, contracts, radiates yet more, and collapses — a positive-feedback radiative collapse [16]. Define the barrier

$$h(\quad x) \;=\; P_{\rm collapse} - P_c(\quad x) \;\ge\; 0, \qquad \mathcal{C} = \{ \quad x : h(\quad x) \ge 0\},$$

so the safe set $\mathcal{C}$ is the region of stable core radiation. With the (surrogate) core-radiation dynamics $\dot{P}_c = L_f P_c(\quad x) + L_g P_c(\quad x)\,\Gamma_{\rm Ar}$, h is a control-barrier function if there exists an admissible seed such that

$$\dot{h} + \alpha(h) \;\ge\; 0 \quad\Longleftrightarrow\quad -L_f P_c - L_g P_c\,\Gamma_{\rm Ar} \;\ge\; -\alpha(h),$$

for a class-$\mathcal{K}$ function α [26]. The guard filters the desired seed $\Gamma^{\rm des}_{\rm Ar}$ from §3.1–3.2 through the minimal-intervention quadratic program

$$\Gamma^{\rm safe}_{\rm Ar} = \arg\min_{\Gamma}\ \tfrac{1}{2}\big(\Gamma - \Gamma^{\rm des}_{\rm Ar}\big)^2 \quad \text{s.t.} \quad L_g P_c\,\Gamma \;\le\; \alpha\big(h(\quad x)\big) - L_f P_c, \quad 0 \le \Gamma \le \Gamma_{\rm max}.$$

Because equation (14) is a scalar QP with one barrier constraint and a box, its solution is the closed-form clip $\Gamma^{\rm safe}_{\rm Ar} = \min\big(\Gamma^{\rm des}_{\rm Ar}, \Gamma_h\big)$ with $\Gamma_h = (\alpha(h) - L_f P_c)/L_g P_c$: the guard passes the controller's request unless it would breach the barrier, in which case it returns the largest seed on the barrier. Forward-invariance follows from the standard CBF theorem: if $x(0) \in \mathcal{C}$ and equation (13) holds for the applied $\Gamma^{\rm safe}_{\rm Ar}$, then $h(\quad x(t)) \ge 0$ for all t — the plasma never leaves the stable-radiation set, and equation (8) is guaranteed, not merely tracked [26]. The guard sits beneath both regulators and above the certified safety clamp; its acceptance test is that no seeding sweep produces a radiative collapse. This is the same maturity-gated, safety-filtered pattern as the Kronos certified control-barrier clamp for the core plasma [34], applied here to the exhaust.

SUPPORTING CONTROLLERS

Two supporting controllers complete the complement. A *strike-point sweeper* distributes the target load and erosion in time; physical-sputtering calculations (serial BR-L2-A27, RustBCA) give a deuterium-on-tungsten peak yield of 1.35×10^{-2} atoms per ion with sub-monolayer-per-pulse net erosion at divertor flux, so sweeping trades a small, well-mapped erosion cost for a large reduction in local peak loading. A *heat-flux limiter* caps the peak wall flux below q_{lim} against a demonstrated thermal margin: the blanket thermal-hydraulics (serial BR-L1-A9) carry 95.2 MW of thermal power with passive decay-heat rejection below 710 °C [32], so the limiter acts against a wall with headroom rather than a bare limit.

CONTROLLER	PHYSICS ANCHOR	CONTROLLED QUANTITY	ACCEPTANCE TEST
detachment-front regulator	UEDGE seeded SOL (BR-L2-A21)	$T_{e,t}$ / front	stays detached
radiated-fraction controller	cooling curves (BR-L2-A29)	f_{rad}	held within tolerance
radiative-collapse guard	core radiation (BR-L2-A30)	P_c	no radiative collapse
strike-point sweeper	sputter/erosion (BR-L2-A27)	target load spread	peak load/erosion cut
heat-flux limiter	blanket margin (BR-L1-A9)	peak $q_{\perp,t}$	below the wall limit

The exhaust control complement, each controller anchored to a demonstrated edge-physics result and gated by an explicit acceptance test. Serials refer to the register [36].

§ 4

Numerical formulation and solvers

THE FINITE-VOLUME EDGE SOLVE

The plant of §2.3 is a converged solution of the Braginskii-class edge fluid equations on a field-aligned mesh. UEDGE [20] advances the coupled continuity, parallel momentum, and electron/ion energy equations in conservative finite-volume form,

$$\frac{\partial U}{\partial t} + \nabla\cdot F(U) = S(U), \qquad U = \left(n,\, nm_iV_\parallel,\, \tfrac{3}{2}nT_e,\, \tfrac{3}{2}nT_i\right),$$

with cross-field diffusive and parallel convective/conductive fluxes F and volumetric sources S for ionisation, recombination, charge-exchange and impurity radiation. Steady state is reached by a fully implicit backward-Euler advance solved at each step by a Newton–Krylov iteration; the Jacobian is formed by numerical perturbation and preconditioned by an incomplete LU factorisation, and convergence is declared when the scaled nonlinear residual falls below 10^{-6}. Boundary conditions are Bohm sheath fluxes at the target with recycling coefficient 0.98, and fixed core-density/temperature at the inner boundary; the three table 1 states differ only in the core-density boundary value. Each point is a true steady state, not a transient snapshot; grid convergence was checked by refining the near-target poloidal spacing until n_t/n_u moved by less than the $15\,\%$ margin to the one-dimensional arbiter.

THE REAL-TIME SAFETY-FILTER QP

The control-side numerics reduce to the scalar QP of equation (14) solved once per control tick. Because a single barrier and a box bound a scalar decision variable, the Karush–Kuhn–Tucker conditions collapse to the closed-form clip given in §3.3; no iterative QP solve is required, and the guard adds only a comparison and a division to the loop, well inside a millisecond budget. The reference-governor arbitration (11) is a two-variable constrained least-squares projection onto the admissible set, solved by an active-set step that is likewise closed-form for the box-and-halfspace geometry here. The PI loops of §3.1–3.2 are discretised by a trapezoidal (Tustin) rule at the control-tick rate with the anti-windup back-calculation applied on saturation.

REDUCED-ORDER CLOSED-LOOP MODEL

The closed-loop demonstrations of §6 integrate a reduced-order model calibrated to the frozen anchors: the first-order front dynamics $\tau_T\dot{T}_{e,t} = -(T_{e,t} - T_{e,t}^{\mathrm{ss}})$ with $T_{e,t}^{\mathrm{ss}} = T_{\mathrm{att}}\exp[-\alpha(\Gamma_{\mathrm{Ar}} - d)]$ anchored to the frozen attached value $T_{\mathrm{att}} = 14.4\,eV$, and the radiated-fraction/core-radiation maps of §3.2–3.3. The ordinary differential equations are advanced by an explicit step at $\Delta t = 0.2\,ms$, two orders of magnitude below τ_T, so the closed-loop trajectories are step-size converged. These are demonstrations of the control laws on the reduced model, not plant measurements; the confirming high-fidelity calculation is the open item of §8.

§ 5

GPU-HPC methodology

Every anchor in this paper was produced by the NVIDIA GPU HPC campaign that underlies the Kronos de-risking programme; the codes run for *this* paper are listed in table 3. The converged edge solve (BR-L2-A21) was run with UEDGE; the impurity cooling curves and the tungsten tolerance (BR-L2-A29) with radas/ColRadPy over ADAS ADF11 atomic data; the physical-sputtering yields for the strike-point sweeper (BR-L2-A27) with the GPU binary-collision code RustBCA cross-checked against SRIM; the double-null heat-flux split (BR-CX-02) with the free-boundary equilibrium solver FreeGS; and the systems/operating-point context and the collapse boundary (BR-L2-A30) with cfspopcon. The reduced 2-D Super-X target-load and neutral/recycling proxies (HX-14, HX-15) and the stacked-lever Monte-Carlo closure ($N = 4000$; BR-SX-09) were run on the same fleet, and the confirming full solve uses SOLPS-ITER [21] (B2.5 coupled to the EIRENE neutral Monte-Carlo [22]), built from source. GPU acceleration serves the campaign in two ways: the many-case parameter scans and Monte-Carlo closures are embarrassingly parallel across the A100/H100/A10 fleet, and the neural surrogates and reduced-order operators that shadow these codes in the control loop are trained and served on the GPU nodes while the fast, analytic control-side numerics of §4 run on the in-house node so the protective loops never contend with the training fleet. All results carry a fixed random seed (20260726) and a recorded toolchain (e.g. SOLPS-ITER 3.2.1a) and are regenerable from the archived drivers; verification is by cross-method agreement — the UEDGE onset ratio $n_t/n_u = 31$ against the one-dimensional arbiter ≈ 27 (within $15\,\%$), and the reduced 2-D proxies against a one-dimensional SD1D cross-check. No compute-cost figures are reported; compute is represented by hardware class only.

CODE	ROLE	ANCHOR / SERIAL	
UEDGE	2-D edge fluid SOL steady states	detachment scan (BR-L2-A21)	
radas / ColRadPy	coronal-equilibrium cooling curves	Ar/W L_z, W tolerance (BR-L2-A29)	
RustBCA / SRIM	binary-collision sputtering/erosion	D→W yield (BR-L2-A27)	
FreeGS	free-boundary equilibrium	double-null heat-flux split (BR-CX-02)	
cfspopcon	0-D systems / operating point	density-limit \	collapse context (BR-L2-A30)
SOLPS-ITER + EIRENE	confirming 2-D edge+neutrals	stacked detachment (HX-14; open)	

Codes run for this paper on the NVIDIA GPU HPC campaign, with the anchor each produced. All are reproduced or derived frozen results in the register [36]; no cost figures are reported.

§ 6

Results

THE ESTABLISHED WINDOW

Sections 2.3–2.5 establish, from converged physics, the window the controllers hold: the target temperature collapses from **14.4** to 1.05 eV across the scan (table 1, figure 2); deuterium alone cannot detach at design exhaust, so seeding is mandatory (figure 3); argon is the edge radiator and core tungsten is capped at $\leq \mathbf{3}$ against a 0.19 MW-per-ppm tolerance (figures 4–5); and Super-X plus double-null geometry walks the peak load toward the 10 MW/m^2 limit and the seed toward the core-tolerable $\leq \mathbf{0.5\,\%}$ (figure 6). These are the frozen results the controllers are built against.

CLOSED-LOOP DETACHMENT HOLD

Figure 8 shows the detachment-front regulator of §3.1 on the reduced-order model. Both loops start detached at the $T^*_{e,t} = 3\,eV$ set-point; at $t = 150\,ms$ a $+35\,\%$ exhaust-power transient is injected. The open loop, holding a fixed seed, reattaches: its target temperature climbs back through the 5 eV threshold toward $\sim 9\,eV$. The closed loop raises the argon command through the PI law (10) with anti-windup and holds the target at 3 eV throughout, never crossing threshold. The regulator meets its acceptance test — stays detached across the disturbance — on the demonstrated model.

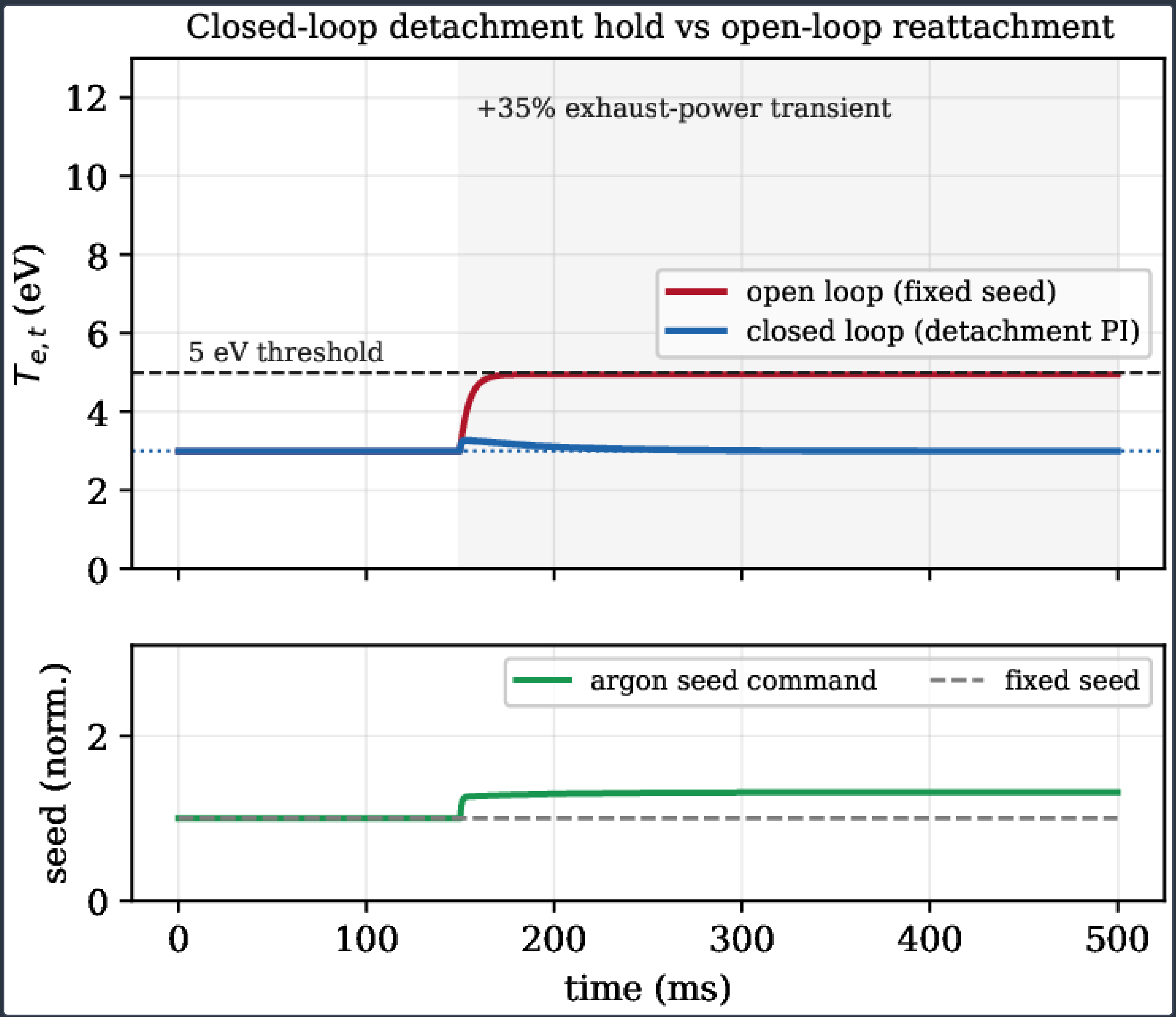

Reduced-order closed-loop simulation of the detachment-front regulator (§3.1), calibrated to the frozen UEDGE anchors. **Top:** target temperature; the open loop (fixed seed) reattaches through the 5 eV threshold after a $+35\,\%$ exhaust-power transient at 150 ms, while the closed loop holds 3 eV. **Bottom:** the argon seed command. Model demonstration, not a plant measurement.

RADIATED-FRACTION TRACKING UNDER THE GUARD

Figure 9 shows the radiated-fraction controller of §3.2 together with the radiative-collapse guard of §3.3. The operator steps the radiated-fraction set-point from 0.75 to 0.92 at $t = 250\,ms$ — a demand for deeper detachment. The controller drives the argon seed up to track it, but the guard's barrier constraint (14) activates as the core radiation P_c approaches the collapse boundary: the guard-applied seed departs from the controller command and saturates exactly on the barrier, holding P_c at the boundary rather than past it, while anti-windup keeps the integrator from winding up behind the saturation. The realised radiated fraction settles just below the raw set-point — the deepest detachment the core-radiation safety constraint allows — and no collapse occurs. This is forward-invariance in action: the guard converts equation (8) from a tracked target into a guaranteed bound.

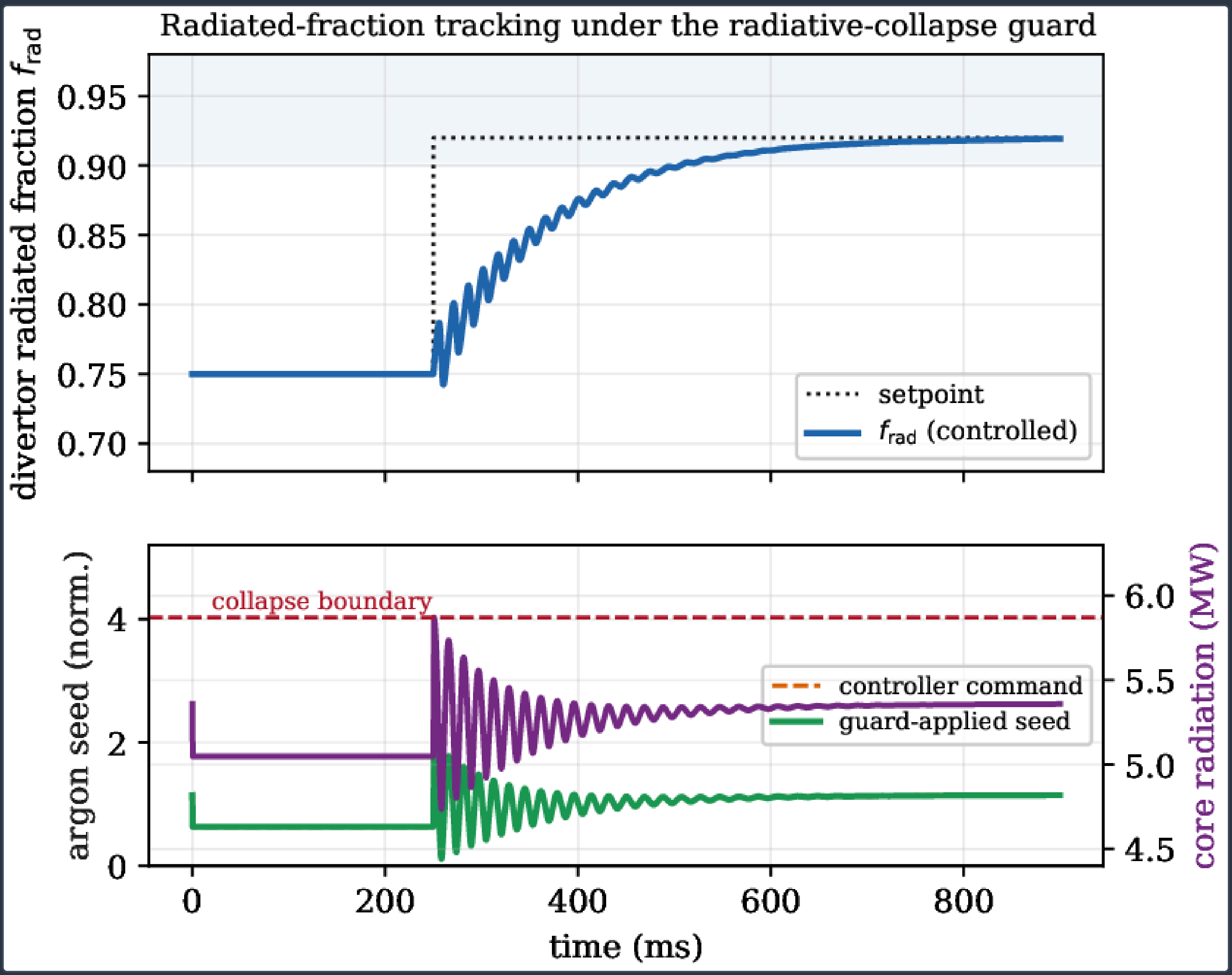

Reduced-order closed-loop simulation of the radiated-fraction controller (§3.2) under the radiative-collapse guard (§3.3). **Top:** the controlled radiated fraction tracks a set-point step, settling just below it where the guard binds. **Bottom:** the controller command (dashed) is clipped by the guard-applied seed (solid) as core radiation (right axis) reaches the collapse boundary (dashed red); the barrier constraint holds P_c on the boundary. Model demonstration.

ACCEPTANCE-CRITERIA STATUS

Table 4 collects the acceptance criteria with their status. The physics anchors (the detachment scan, cooling curves, tungsten tolerance, heat-flux ladder, sputter yields) are reproduced or derived frozen results; the controller acceptance tests are demonstrated on the reduced-order model calibrated to those anchors, and are pre-registered targets for the confirming high-fidelity solve. Nothing here is claimed as a plant measurement.

CRITERION	BASIS	STATUS
target-temperature collapse 14.4 → 1.05 eV	UEDGE (BR-L2-A21)	frozen
onset $n_t/n_u = 31$ vs arbiter ≈ 27 ($< 15\%$)	UEDGE + 1-D arbiter	frozen
seeding mandatory at design $q_{\parallel}$	two-point scaling (BR-L2-A21)	frozen
argon edge/core contrast $\sim 13\times$; W ≤ 3 ppm	radas/ADAS (BR-L2-A29)	frozen
peak load $\rightarrow \leq 10$ MW m^{-2}; seed $\rightarrow \leq 0.5\%$	HX-14 / BR-CX-02 / A11-SUM	frozen
detachment held across $+35\%$ transient	front regulator, reduced model	model-demonstrated
f_{rad} held; no radiative collapse	guard QP, reduced model	model-demonstrated
full 2-D SOLPS-ITER confirmation	SOLPS-ITER + EIRENE	**open**

Acceptance criteria, targets and status. “Frozen” denotes a reproduced/derived register result; “model-demonstrated” denotes a reduced-order closed-loop result calibrated to the frozen anchors; the confirming 2-D SOLPS-ITER solve is the open item (§8).

§ 7

Discussion

AGAINST THE PUBLISHED DETACHMENT-CONTROL LITERATURE

The controllers here are built on, and are complementary to, the established real-time detachment-control results. Kallenbach *et al.* closed a divertor power-load loop with nitrogen seeding on ASDEX Upgrade and set out the seeding-based exhaust strategy from present devices to DEMO [13,12]; our contribution differs in the actuator target (argon on a Super-X leg, chosen for the $\sim 13\times$ edge/core cooling contrast of figure 4) and, decisively, in adding a certified safety filter beneath the loop. Ravensbergen *et al.* regulated the impurity emission-front position on TCV with tens-of-millisecond response [14]; our front regulator adopts the same first-order plant and response class (figure 8) and augments it with the two-point-model feedforward of equation (9), which is what keeps the loop stable as the plant grows seed-sensitive near onset. Verhaegh *et al.* established the detachment physics of a genuine Super-X divertor on MAST Upgrade [15]; our plant is a converged Super-X SOL solve for the breeder design point, and the $n_t/n_u = 31$ onset with a $T_{e,t} < 5\,eV$ target is consistent with the strong-detachment, low-target-temperature regime those experiments reach. The novel element relative to all three is the radiative-collapse guard: casting core-radiation protection as a control-barrier QP (equations 12–14) turns the “do not over-seed” operating heuristic into a forward-invariance guarantee [26], with the shared-actuator arbitration handled by a reference governor [27].

AGAINST THE IMPURITY-TOLERANCE LITERATURE

The tungsten guard of §2.4 is consistent with the community's consolidated impurity-tolerance analysis. P\"utterich *et al.* evaluated tolerable impurity concentrations for a reactor plasma from a consistent set of cooling factors, finding tungsten tolerable only at the few-parts-per-million level and argon a viable seeded radiator at the sub-percent level [16]; our frozen anchors — core tungsten capped at ≤ 3 and a core-tolerable argon seed of $\leq 0.5\,\%$ (figures 5, 6) — fall squarely inside that envelope, and the 0.19 MW-per-ppm tungsten sensitivity is the quantitative rule the radiated-fraction controller enforces. The reduced-model target-temperature threshold $T_{\mathrm{det}} \approx 5\,eV$ and the momentum-loss rollover are those of Stangeby's reduced detachment models [9] and the ultimate-detachment picture of Krasheninnikov and Kukushkin [11]; the near-SOL width scaling that drives the large $q_\parallel$ is the Eich/Goldston result [6,7]. In short, the physics anchors sit inside the published ranges, and the paper's contribution is the control architecture that holds the plasma inside them.

WHY THE GUARD MATTERS FOR A COMPACT BREEDER

In a compact ST breeder the argument for the guard is sharper than in a research tokamak. The core radiation budget is small (4.670 MW) against a fusion power of 85.04 MW, and the same argon valve sets both the detachment depth and the core impurity load; a controller optimising detachment alone can walk the core toward collapse without any single command looking unsafe. The CBF guard makes the safe set forward-invariant regardless of what the detachment and radiated-fraction loops request, so the aggressive seeding needed to hold a narrow detached window on a high-$q_\parallel$ device is bounded by a guarantee rather than by operator caution. This is the exhaust-side instance of the maturity-gated, safety-filtered control philosophy applied across the Kronos breeder control suite [35].

§ 8

Limitations

One honest gate bounds the claims. The detachment window rests on a converged but reduced edge solve — UEDGE with diffusive neutrals and analytic rates — which is a trustworthy *trend* instrument, and its onset ratio agrees with an independent one-dimensional arbiter to within 15 %, but the absolute-threshold arbiter is the fully two-dimensional SOLPS-ITER solve coupled to EIRENE neutrals. That solve is built (geometry and full deck) but its convergence is grid-topology-blocked for the stacked Super-X geometry, so no first-principles 2-D detachment number is quoted here (nothing is fabricated); the present UEDGE result and the one-dimensional arbiter bracket its expected answer, and it is the one open confirming calculation. The closed-loop results of §6 are correspondingly reduced-order demonstrations of the control laws on a model calibrated to the frozen anchors, not plant or hardware measurements; hardware-in-the-loop confirmation on the digital twin, then the plant, is the gate to full control authority.

§ 9

Conclusion

Detachment is mandatory for the compact ST breeder, seeding is mandatory to reach it, and holding it is a control problem with a safety core. A converged UEDGE scan drives the breeder Super-X target from $\mathbf{14.4}$ to 1.05 eV with an onset ratio $n_t/n_u = \mathbf{31}$ agreeing with a one-dimensional arbiter to $\mathbf{15}\,\%$, and the two-point-model scaling shows deuterium alone cannot detach at the design $q_{\|} \simeq 12\,GW/m^2$, placing the deuterium-only threshold at one-to-two times Greenwald. Coronal cooling curves make argon the edge radiator (a $\sim\mathbf{13}\times$ core-to-edge contrast) and cap core tungsten at $\leq \mathbf{3}$ against a 0.19 MW-per-ppm tolerance, and Super-X plus double-null geometry walks the peak load toward the 10 $\mathrm{MW/m^2}$ limit and the seed toward a core-tolerable $\leq \mathbf{0.5}\,\%$. On this demonstrated window we specify three coupled controllers — a detachment-front regulator with two-point-model feedforward, a radiated-power-fraction controller, and a radiative-collapse guard cast as a control-barrier quadratic program that renders the core-radiation safe set forward-invariant — and demonstrate on a reduced-order model calibrated to the frozen anchors that the regulator holds detachment through a $+\mathbf{35}\,\%$ transient that reattaches the open loop, and the guard caps an over-seed command exactly at the collapse boundary. The breeder's exhaust is a controlled, protected state with a quantified physics basis; the one open item is the fully two-dimensional SOLPS-ITER confirmation, which the present results bracket.

Acknowledgments tocsectionAcknowledgments Part of the Kronos Fusion Energy 2026 design series. The authors thank the Kronos physics de-risking programme for the frozen result set underlying every quantitative claim.

Reproducibility. The detachment scan (BR-L2-A21, UEDGE), impurity cooling curves and tungsten tolerance (BR-L2-A29, radas/ColRad-Py), double-null heat-flux split (BR-CX-02, FreeGS), Super-X target-load proxy (HX-14), stacked-lever closure (BR-SX-09), sputter yields (BR-L2-A27, RustBCA), and blanket thermal margin (BR-L1-A9) are frozen results in the Kronos Physics De-Risking Register [36], regenerable from the archived drivers with fixed seed 20260726; the reduced-order closed-loop figures are regenerable from the figure-generation script deposited with this paper. This paper is archived at its DOI doi:10.5281/zenodo.22645874; official version: https://www.kronosfusionenergy.com/publications/real-time-detachment-control-for-a-super-x-divertor-in-.html and its official page https://www.kronosfusionenergy.com/publications/real-time-detachment-control-for-a-super-x-divertor-in-.html; the de-risking register is doi:10.5281/zenodo.22133057.

Data availability tocsectionData availability The edge-solve outputs, cooling-curve anchors, heat-flux and seed ladders, and the reduced-order closed-loop trajectories used for the figures are archived with the deposit at doi:10.5281/zenodo.22645874, which references the Kronos 2026 series register doi:10.5281/zenodo.22133057 and the AI/quantum-control paper doi:10.5281/zenodo.21842371. All quantitative values trace to the register by the serial identifiers cited inline. Any economic analysis is reported separately and is not part of the public deposit.

Competing interests tocsectionCompeting interests Provisional patent applications relating to aspects of this work have been filed.

tocsectionReferences

APPARATUS

Portfolio, People & Record

The intellectual-property estate, the people who built it, the limitations that gate it, and the sources it rests on.

1	4	40	27
GRANTED PATENT	2026 PROVISIONALS	TEAM MEMBERS	2022 PROVISIONALS

INTELLECTUAL PROPERTY

The patent portfolio

The estate spans a granted high-field magnet patent, pending utility and 2026 provisional filings that map to the two products, a digital-twin control provisional, a registered trademark application, and the original 2022 provisional family. Every patentable disclosure in the five-paper arXiv drop was protected **before** publication: the breeder and burner provisionals were filed 1–2 August, and a publication-gap omnibus filing the evening before the drop swept up the DEC, plasma-control, and REBCO-winding matter of the three otherwise-unprotected papers. Patent numbers and application serials are matters of public record; claim scope is summarised, not reproduced.

GRANTED & PENDING UTILITY

US 12,009,112	High-field tilted graded-REBCO magnet architecture (KRONO-002A) · *app. 17/878,550*	GRANTED
US 17/878,507	Core device / method (KRONO-001A) · *utility*	PENDING

2026 PROVISIONAL FILINGS — MAPPED TO THE PRODUCTS

64/124,209	Hyperion — spherical-tokamak tritium / helium-3 foundry · *breeder · filed Aug 2026*	FILED
64/124,220	Aegis / MetroVolt — synchrotron-cutoff, fuel-selection & plug-winding · *generator · filed Aug 2026*	FILED
64/115,167	KRONOS-CTRL digital-twin plant control · *provisional · filed Jul 2026*	FILED
64/005,440	Integrated spherical-tokamak fusion architecture · *early integrated-architecture filing · filed Mar 2026*	FILED
64/105,530	Negative-triangularity spherical-tokamak architecture · *foundational ST filing · filed Jul 2026*	FILED
64/128,097	Publication-gap omnibus — quasineutral two-species expander DEC · provenance-gated / latency-split plasma control · as-built high-field winding & conductor architecture · *filed 7 Aug 2026, the evening before the arXiv drop*	FILED

TRADEMARK & ORIGIN

FTK-98801894	Kronos Fusion Energy — trademark application	FILED
KR-2022-*	Original provisional family (KR-2022-00001 … 00027) · *27 filings, 2022*	PRIORITY

The narrow, defensible magnet novelty — the specific conductor and the digital-twin winding optimisation, not high-field REBCO as a category — is the commercial core that can earn ahead of any Q > 1 milestone, with markets in fusion magnet supply, MRI/NMR, accelerators, and proton therapy. The claim is scoped honestly: the high field is a *system field* result, not a stand-alone-coil record; the small-bore plug coil is structurally infeasible as a bare winding but resolved by a stress-managed structural shield (feasible-pending-FEA); and the winding-tape experiment returned a *null result*. The value is the method, not a field record.

THE TEAM

Founding partners, board, advisors & auditors

Kronos is built by a bench of advanced-fuel-fusion, high-field-magnet, direct-conversion, and materials specialists, with a board and operations team drawn from defense, national laboratories, and industry. Dates are shown as ranges; where a tenure has ended or is term-ending, the range says so.

FOUNDING PARTNERS — SCIENCE

Dr. Gerald Kulcinski
Co-Founder · Helium-3 & Advanced-Fuel Fusion
UW–Madison · 2023–Present

Dr. Carl Weggel
Chief Scientist / S.M.A.R.T. Design
MIT Alcator Program · 2022–Present

Dr. Robert J. Weggel
Magnetic Field Design
MIT Magnet Lab · 2022–Present

BOARD

Priyanca Ford
Founder & CEO · Executive Board
2022–Present

Bandel Carano
Finance / Strategy
Oak Investment Partners / Stanford · 2025–2026

Patrick Schweiger
Fusion Device Engineering
Oklo / CFS / TerraPower · 2025–Present

SCIENTIFIC ADVISORS

Dr. Steven O. Dean
Fusion Policy & History
DOE / Fusion Power Associates · 2025–Present

Dr. Patrick H. Diamond
Plasma Turbulence & Transport
UC San Diego · 2025–Present

Dr. Jack J. Dongarra
HPC & Numerical Algorithms
Turing Award · 2025–Present

Dr. Nasr M. Ghoniem
Chief Material Scientist
UCLA · 2025–Present

Dr. Siegfried Glenzer
Plasma Physics & Laser Fusion
Stanford / SLAC · 2022–Present

Dr. David A. Hammer
Pulsed-Power Fusion
Cornell · 2025–Present

Dr. Donald A. Spong
Plasma Theory & Confinement
ORNL · 2025–Present

Dr. Curtis Smith
Risk Assessment & Nuclear PRA
MIT / Idaho National Lab · 2025–Present

RADM (Ret.) David Goggins
Naval Engineering & Power-Plant Design
U.S. Navy · 2023–2026

Dr. Konstantin Batygin
Mathematician
Caltech · 2022–2025

Dr. Ruben Fair
Magnet Design / ITER Liaison
PPPL / Jefferson Lab · 2022–2025

Dr. Paul S. Weiss
Materials & Nanotechnology
UCLA · 2022–2025

SCIENTIFIC AUDITORS

Dr. Wilfred A. Cooper
Plasma Equilibrium Theory
EPFL / Swiss Plasma Center · 2025–Present

Dr. Ahmed Hassanein
Plasma–Material Interactions
Purdue / Argonne · 2025–Present

Dr. Patrick E. Hopkins
Extreme Thermal Materials
U. of Virginia · 2025–Present

Dr. Peter Hosemann
Materials Joining & Structural Integrity
UC Berkeley · 2025–Present

Dr. Travis W. Knight
Advanced Nuclear Fuels & Systems
U. of South Carolina · 2025–Present

Dr. Philippe Lebrun
Cryogenics & Magnet Cooling
CERN · 2025–Present

Dr. Nitendra Singh
Nuclear Safety & Fuel Cycle
ITER · 2025–Present

Dr. Guido Van Oost
Magnetic Confinement & Fusion Systems
Ghent University · 2025–Present

Dr. Gary S. Was
Radiation Materials & Structural Integrity
U. of Michigan · 2025–Present

Dr. Ray Sedwick
Direct Energy Conversion
U. of Maryland · 2025

OPERATIONS

Michael Laughlin
Chief Operating Officer
2022–Present

Martin Owens
Chief Strategy Officer
LANL / GE Hitachi · 2022–Present

MG (Ret.) Paul Pardew
Chief Contracting Officer
Army Contracting Command · 2022–Present

David Beck
Fusion Commercialization
U.S. Space Force · 2024–Present

Sushma Bhatia
Environmental & Legislative
Google · 2022–Present

Michael De Frenza
Technology Licensing
2023–Present

MG (Ret.) Robin L. Fontes
Cybersecurity & Defense
Army Cyber Command · 2022–Present

Vijay Gehani
Supply Chain & Components
INOX India · 2024–Present

Jon Michel Greenwood
IT & AI Infrastructure
Live Nation · 2023–Present

Brian C. O'Neill
National Security
CIA / ODNI · 2022–Present

Gen. (Ret.) Gustave F. Perna
DoD Liaison
Operation Warp Speed · 2022–2023

Andrea Romero
Marketing Lead
2022–Present

Legal counsel is retained; those roles are held on the internal roster and are not listed here.

SOURCES

References

1 J E Menard *et al*, Fusion nuclear science facilities and pilot plants based on the spherical tokamak, *Nucl. Fusion* **56** 106023 (2016). doi:10.1088/0029-5515/56/10/106023

2 B N Sorbom *et al*, ARC: a compact, high-field, fusion nuclear science facility and demonstration power plant with demountable magnets, *Fusion Eng. Des.* **100** 378 (2015). doi:10.1016/j.fusengdes.2015.07.008

3 A J Creely *et al*, Overview of the SPARC tokamak, *J. Plasma Phys.* **86** 865860502 (2020). doi:10.1017/S0022377820001257

4 M E Austin *et al*, Achievement of reactor-relevant performance in negative triangularity shape in the DIII-D tokamak, *Phys. Rev. Lett.* **122** 115001 (2019). doi:10.1103/PhysRevLett.122.115001

5 A Marinoni, O Sauter and S Coda, A brief history of negative triangularity tokamak plasmas, *Rev. Mod. Plasma Phys.* **5** 6 (2021). doi:10.1007/s41614-021-00054-0

6 T Eich *et al*, Scaling of the tokamak near the scrape-off layer H-mode power width and implications for ITER, *Nucl. Fusion* **53** 093031 (2013). doi:10.1088/0029-5515/53/9/093031

7 R J Goldston, Heuristic drift-based model of the power scrape-off width in low-gas-puff H-mode tokamaks, *Nucl. Fusion* **52** 013009 (2012).

8 P C Stangeby, *The Plasma Boundary of Magnetic Fusion Devices* (Bristol: IOP Publishing, 2000).

9 P C Stangeby, Basic physical processes and reduced models for plasma detachment, *Plasma Phys. Control. Fusion* **60** 044022 (2018). doi:10.1088/1361-6587/aaacf6

10 C S Pitcher and P C Stangeby, Experimental divertor physics, *Plasma Phys. Control. Fusion* **39** 779 (1997).

11 S I Krasheninnikov and A S Kukushkin, Physics of ultimate detachment of a tokamak divertor plasma, *J. Plasma Phys.* **83** 155830501 (2017). doi:10.1017/S0022377817000654

12 A Kallenbach *et al*, Impurity seeding for tokamak power exhaust: from present devices via ITER to DEMO, *Plasma Phys. Control. Fusion* **55** 124041 (2013). doi:10.1088/0741-3335/55/12/124041

13 A Kallenbach *et al*, Divertor power load feedback with nitrogen seeding in ASDEX Upgrade, *Plasma Phys. Control. Fusion* **52** 055002 (2010).

14 T Ravensbergen, M van Berkel, A Perek *et al*, Real-time feedback control of the impurity emission front in tokamak divertor plasmas, *Nat. Commun.* **12** 1105 (2021). doi:10.1038/s41467-021-21268-3

15 K Verhaegh *et al*, The role of plasma–atom and molecule interactions on power & particle balance during detachment on the MAST Upgrade Super-X divertor, *Nucl. Fusion* **63** 126023 (2023). doi:10.1088/1741-4326/acf946

16 T P\"utterich *et al*, Determination of the tolerable impurity concentrations in a fusion reactor using a consistent set of cooling factors, *Nucl. Fusion* **59** 056013 (2019). doi:10.1088/1741-4326/ab0384

17 H P Summers *et al*, Ionization state, excited populations and emission of impurities in dynamic finite density plasmas (ADAS), *Plasma Phys. Control. Fusion* **48** 263 (2006).

18 D E Post, A review of recent developments in atomic processes for divertors and edge plasmas, *J. Nucl. Mater.* **220–222** 143 (1995).

19 L L Lengyel, *Analysis of radiating plasma boundary layers*, Max-Planck-Institut f\"ur Plasmaphysik Report IPP 1/191 (1981).

20 T D Rognlien, J L Milovich, M E Rensink and G D Porter, A fully implicit, time-dependent 2-D fluid code for tokamak edge plasmas (UEDGE), *J. Nucl. Mater.* **196–198** 347 (1992).

21 S Wiesen *et al*, The new SOLPS-ITER code package, *J. Nucl. Mater.* **463** 480 (2015). doi:10.1016/j.jnucmat.2014.10.012

22 D Reiter, M Baelmans and P B\"orner, The EIRENE and B2-EIRENE codes, *Fusion Sci. Technol.* **47** 172 (2005).

23 L L Lao, H St John, R D Stambaugh, A G Kellman and W Pfeiffer, Reconstruction of current profile parameters and plasma shapes in tokamaks, *Nucl. Fusion* **25** 1611 (1985). doi:10.1088/0029-5515/25/11/007

24 F Felici *et al*, Real-time physics-model-based simulation of the current density profile in tokamak plasmas, *Nucl. Fusion* **51** 083052 (2011). doi:10.1088/0029-5515/51/8/083052

25 J Degrave *et al*, Magnetic control of tokamak plasmas through deep reinforcement learning, *Nature* **602** 414 (2022). doi:10.1038/s41586-021-04301-9

26 A D Ames, X Xu, J W Grizzle and P Tabuada, Control barrier function based quadratic programs for safety critical systems, *IEEE Trans. Autom. Control* **62**(8) 3861 (2017). doi:10.1109/TAC.2016.2638961

27 E Garone, S Di Cairano and I Kolmanovsky, Reference and command governors for systems with constraints: a survey on theory and applications, *Automatica* **75** 306 (2017). doi:10.1016/j.automatica.2016.08.013

28 M V Kothare, P J Campo, M Morari and C N Nett, A unified framework for the study of anti-windup designs, *Automatica* **30** 1869 (1994).

29 P I Ford and G L Kulcinski, *A Stacked Detachment Portfolio for a Compact Spherical-Tokamak Breeder: Super-X, Double-Null and Snowflake Geometries that Cut the Required Argon Seed Fraction*, Kronos Fusion Energy 2026 series. doi:10.5281/zenodo.22645742. Official page https://www.kronosfusionenergy.com/publications/divertor-portfolio.html

30 P I Ford and G L Kulcinski, *Collisional-Radiative Impurity-Radiation Modeling for a Compact Spherical-Tokamak Breeder: Closing the Core and Edge Radiated-Power Budget*, Kronos Fusion Energy 2026 series. doi:10.5281/zenodo.22645883. Official page https://www.kronosfusionenergy.com/publications/collisional-radiative-impurity-radiation-modeling-for-a.html

31 P I Ford, *The Greenwald-Fraction Density Limit and the Radiative Boundary: Mapping the Safe Operating Envelope of a Compact Spherical-Tokamak Breeder*, Kronos Fusion Energy 2026 series. doi:10.5281/zenodo.22645947. Official page https://www.kronosfusionenergy.com/publications/the-greenwald-fraction-density-limit-and-the-radiative-.html

32 P I Ford and G L Kulcinski, *Blanket and Divertor Thermal-Hydraulics for a Compact Spherical-Tokamak Breeder: Coolant Heat Removal, Peak-Temperature Margins, and the Walk-Away Safety Case*, Kronos Fusion Energy 2026 series. doi:10.5281/zenodo.22645836. Official page https://www.kronosfusionenergy.com/publications/blanket-and-divertor-thermal-hydraulics-for-a-compact-s.html

33 P I Ford and G L Kulcinski, *A Flowing-Lithium Vapor-Box Divertor with Molten-Salt In-Loop Tritium Extraction for a Compact Spherical-Tokamak Breeder*, Kronos Fusion Energy 2026 series. doi:10.5281/zenodo.22645750. Official page https://www.kronosfusionenergy.com/publications/flowing-lithium-vapor-box-divertor.html

34 P I Ford, *A Certified Control-Barrier Safety Filter for Fusion Control: Forward-Invariance Guarantees, Calibrated Uncertainty, and an Honest PINN Negative for a Compact Spherical-Tokamak Breeder*, Kronos Fusion Energy 2026 series. doi:10.5281/zenodo.22645716. Official page https://www.kronosfusionenergy.com/publications/control-barrier-safety-clamp.html

35 P I Ford, *A Real-Time Control Suite for a Compact Negative-Triangularity Spherical-Tokamak Breeder: Profile, Shape, Vertical-Stability, q-Profile, and Solenoid-Free Ramp Controllers*, Kronos Fusion Energy 2026 series. doi:10.5281/zenodo.22645809. Official page https://www.kronosfusionenergy.com/publications/a-real-time-control-suite-for-a-compact-negative-triang.html

36 P I Ford, *Kronos Physics De-Risking Register*, Kronos Fusion Energy 2026 series. doi:10.5281/zenodo.22133057

37 P I Ford, *AI and quantum computing for fusion*, Kronos Fusion Energy 2026 design series. doi:10.5281/zenodo.21842371

COLOPHON

How this document was made

The Kronos Fleet — Combined Editorial, 2026 is set in **Fraunces** (display), **Gelasio** (text), and **IBM Plex Mono** (data & equations), carried forward from the Kronos editorial design system.

The figures are rendered at 300 dpi from the deposited generator scripts; the document is composed as a single self-contained file with embedded fonts and imagery, paginated to US Letter, and rendered to PDF through a headless Chromium engine in matched light and dark editions.

Every headline quantity carries an evidence class; withdrawn and restated values are marked as such. Nothing herein is frozen beyond the founder-approved Tier-A set.

Explore it live — turn the interactive 3-D model, run the deposited solvers in the physics validator, and watch the companion film series.

LEGAL NOTICE

Notice, status, and distribution

Conceptual design & simulation study. This document reports a conceptual design and simulation study. It is not a construction commitment, a safety-analysis report, a regulatory filing, or an offer of securities. Forward-looking statements — schedules, costs, market sizes, and performance — are estimates subject to the limitations set out in the Simulations part and may change.

Numbers and their classes. Quantities are reported with evidence classes and case labels; modelled, assumed, and requirement-class values are identified as such and are not to be quoted without their labels.

Public edition. This edition carries the physics and design only; all financial, funding, and defense-commercial content has been removed for public distribution. The scientific text corresponds to the arXiv and journal submissions.

THE 2026 KRONOS SERIES

One programme, many papers

This editorial is one paper in the Kronos 2026 series — a real fusion company's complete, reproducible physics record for a spherical-tokamak breeder and its low-neutron D–^{3}He tandem-mirror burners. Every headline number is a frozen anchor in the Physics De-Risking Register.

Explore the whole programme: the De-Risking Register, the interactive 3-D model, and the physics validator.

KRONOS FUSION ENERGY

Real-Time Detachment Control for a Super-X Divertor in a Compact Spherical-Tokamak Breeder: Radiated-Power-Fraction Regulation with a Radiative-Collapse Guard

A real fusion company building real machines. Explore the science, live.

Zenodo · doi:10.5281/zenodo.22645874

Read on kronosfusionenergy.com

The Physics De-Risking Register